New 40Ar/39Ar age constraints on the Late Palaeozoic tectonic evolution of the western Tianshan (Xinjiang, northwestern China), with emphasis on Permian fluid ingress

Koenraad de Jong, Bo Wang, Michel Faure, Liangshu S. Shu, Dominique Cluzel, Jacques Charvet, Gilles Ruffet, Yan Chen

New $^{40}Ar/^{39}Ar$ age constraints on the Late Palaeozoic tectonic evolution of the western Tianshan (Xinjiang, northwestern China), with emphasis on Permian fluid ingress

Koen de Jong[1] , Bo Wang[1, 2], Michel Faure[1], Liangshu Shu[2], Dominique Cluzel[1], Jacques Charvet[1], Gilles Ruffet[3] and Yan Chen[1]

(1) Institut des Sciences de la Terre d'Orléans, UMR CNRS 6113, Université d'Orléans, Bâtiment Géosciences, 45067 Orléans Cedex 2, France
(2) Department of Earth Sciences, Nanjing University, 210093 Nanjing, China
(3) Géosciences Rennes, UMR CNRS 6118, Université de Rennes 1, Rennes, France

Abstract Laser-probe dating of mylonite whole-rock samples from the North Tianshan—Main Tianshan fault zone that cross-cuts the North Tianshan domain's southern margin yielded $^{40}Ar/^{39}Ar$ spectra with 255–285 Ma ages. Biotite from an undeformed, Early Carboniferous granite, which cuts the steep mylonitic foliation in the Proterozoic basement of the Yili arcs's southern margin, gave a 263.4 ± 0.6 Ma plateau age (1σ). Pre-Carboniferous metasediments overlying this basement yielded plateau ages (1σ) of 253.3 ± 0.3 (muscovite) and 252.3 ± 0.3 (biotite) Ma. The Permian ages of mylonites date movement on these ductile, dextral strike-slip shear zones, whereas the mica ages are interpreted by recrystallisation as a result of fluid flow around such transcurrent faults. We propose that the Tianshan's Permian syn-tectonic bimodal magmatism was created in a non-plume-related Yellowstone-like extensional–transtensional tectonic regime. Gold mineralisation, tracing aqueous flow in the crust, peaked in Permian time and continued locally into the Triassic. The picture is emerging that a convective fluid system partly driven by magmatic heat, existed in a strongly fractured and weakened crust with an elevated heat flow, leading to regional-scale isotope resetting. We suggest that surprisingly young isotopic ages in the literature for early orogenic (ultra)high-pressure metamorphism are similarly due to fluid-mediated recrystallisation.

Keywords $^{40}Ar/^{39}Ar$ geochronology - Isotope resetting - Fluids - Central Asia - Chinese Tianshan

Introduction

The impressive Tianshan is amongst the largest mountain systems in Asia. The up to ca. 400 km wide and 3,500 km long mountain range is situated between the Tarim and Junggar basins and the Kazakh Platform (Fig. 1), and stretches westerly from the Xinjiang Uyghur Autonomous Region of northwestern China to Kazakhstan, Kyrgyzstan and Tajikistan, to terminate farther westward in north-central Uzbekistan. The present-day Tianshan was formed by Cenozoic intraplate deformation in response to the progressive collision of India with Eurasia that continues today as the Himalayan orogeny, as first proposed by Molnar and Tapponnier (*1975*). During this process the heterogeneous Asian continental lithosphere responded by rigid-plastic behaviour; crustal shortening provoked lateral displacement of rigid continental blocks, thereby reactivating Palaeozoic orogens around and sutures between them, as is the case for the Tianshan belt (e.g. Windley et al. *1990*; Poupinet et al. *2002*).

The Palaeozoic Tianshan is a major element of the southern Central Asian Orogenic Belt. The latter is situated between the Siberian craton to the north and Tarim and North China cratons to the south, and extends from the Urals in the west to Sikhote-Alin' in the Russian Far East,

where it is truncated by Pacific subduction-accretion systems of Mesozoic age (Fig. 1, insert). This vast orogenic belt formed in the Palaeozoic due to the closure of Palaeo-Asian oceanic basins and accompanying prolonged accretion of oceanic plate sediments, oceanic crust, including oceanic islands, forearc and backarc basins, and magmatic arcs, as well as by amalgamation of terrains, including Gondwana- and Siberia-derived microcontinents with their passive margins (Filippova et al. *2001*; Dobretsov *2003*; Xiao et al. *2003*, *2004*; Buslov et al. *2004*; Jahn *2004*; Yakubchuk *2004*; de Jong et al. *2006*; Volkova and Sklyarov *2007*; Windley et al. *2007*; and references in these papers). Plate convergence was accompanied by intense arc magmatism and volcanism with a high mantle component (Jahn *2004*). The Tarim craton docked with the Siberian continent's southern active margin during the Mid Permian (Cocks and Torsvik *2007*). This agrees with the observed intermixing of floras typical for Siberia and Tarim in the early Late Permian (Li and Wu *1996*). This points to disappearance of important oceanic basins between these cratons at about 260–255 Ma, according to the time scale of Gradstein et al. (*2004*). The Kazakhstan composite continent appears to have amalgamated with Siberia and Europe before the earliest Triassic (Lyons et al. *2002*).

In Permian time, crustal deformation was partitioned into vertical, ductile, strike-slip shear zones that often reactivated older sutures (Allen et al. *1995*; Buslov et al. *2004*; Laurent-Charvet et al. *2003*). Pull-apart basins underlain by thinned crust were formed in this regional scale transcurrent tectonic regime (Allen et al. *1995*; Wang et al. *2003*; Charvet et al. *2007*; Wang et al. *2008a*, this issue). In rare cases such basins may be characterised by deep-marine sedimentation on a pillow basalt substratum (Shu et al. *2005*). Emplacement of voluminous granites of the alkaline and peralkaline series, as well as mafic-ultramafic intrusives and their volcanic equivalents affected the entire belt across terrane boundaries, starting in earliest Permian time (Coleman *1989*; Allen et al. *1995*; Chen and Jahn *2004*; Jahn *2004*; Chen and Arakawa *2005*; Pirajno et al. *2008*). At least part of the Permian magmatic complexes were emplaced along major strike-slip shear zones that provided suitable conduits for ascending asthenospheric material and heat influx in the crust (Konopelko et al. *2007*; Wang et al. *2008a*, this issue). Similarly, part of the Late Palaeozoic mineralisations occurred closely related to such transcrustal shear zones in which permeability is structurally enhanced, thus providing principal pathways for regional fluid flow (Yakubchuk et al. *2002*; Mao et al. *2004b*, *2005*). The Tianshan in China and the adjacent central Asian republics of the former Soviet Union hosts some of the world's largest gold deposits (Konopelko et al. *2007*; Rui et al. *2002*; Yakubchuk et al. *2002*; Mao et al. *2004b*, *2005*; Zhang et al. *2008a*). Auriferous quartz veins are tracers of high-flux aqueous flow in the crust (Sibson *2007*). Epizonal gold-quartz deposits are generally formed at depths <1–2 km in extensional–transtensional tectonic regimes with concurrent felsic magmatism, where large fluid volumes of predominantly meteoric water may be circulated by convective flow (Sibson *2007*).

In order to place further age constraints on the late Palaeozoic tectonic evolution of the Tianshan Belt in the Xinjiang region and to shed more light on the importance of the Permian magmatic and thermal event and the associated regional-scale fluid flow, we used an $^{40}Ar/^{39}Ar$ laser probe to isotopically date rocks from the array of Permian strike-slip faults and the adjacent zones (Figs. 1, 2) with steeply dipping tectonic fabrics, in which Permian aged granites have intruded. We concentrated on zones that cross cut the southern margin of the Yili block or are located between the latter and the North Tianshan domain (Fig. 1). The results of detailed field observations and structural analyses, as well as geochemistry in these target areas have been published elsewhere (Wang et al. *2006*, *2007b*, *2008a*, *b*, *c*). We advocate that fluid-mediated recrystallisation of mica may lie behind our finding of young (Permian) $^{40}Ar/^{39}Ar$ ages. Further elaborating on a discussion by Gao et al. (*2006*), a similar

mechanism may help to explain recently published unrealistically young isotopic ages for early orogenic high-pressure metamorphism that would imply that this event is as young as the final stages of gold mineralisations, which occurred by convective predominantly, low temperature meteoric fluids, well after suturing.

The Chinese Tianshan Belt

Tectonic units

The Chinese Tianshan belt is subdivided into a number of major tectonic units, the boundaries of which are formed by Late Palaeozoic to Early Mesozoic crustal scale strike-slip faults and Cenozoic thrusts that have strongly modified the original architecture of the orogen (Windley et al. *1990*; Allen et al. *1995*; Shu et al. *1999*; Laurent-Charvet et al. *2003*; Zhao et al. *2003*; Wang et al. *2006*, *2007a*, *b*, *2008a*, *b c*; Charvet et al. *2007*). The belt is usually subdivided into three domains, namely, the North Tianshan, Central Tianshan and South Tianshan (Ma et al. *1993*), but the detailed definition of each domain and their boundaries are still under discussion. A similar tripartition used for the Uzbek and Kyrgyz parts of the Tianshan does not coincide exactly with that used for the Chinese part (see review by Chiaradia et al. *2006*). Additionally, on the basis of new field observations in combination with reassessment of geological maps of the Xinjiang Bureau of Geology and Mineral Resources (XBGMR *1993*) and a review of both Chinese and international literature, Wang et al. (*2008b*) proposed to subdivide the Chinese belt into five domains, from north to south: North Tianshan, Bole block, Yili block, Central Tianshan and South Tianshan. Some of these domains are separated by suture zones that contain ophiolite (mélanges) (Fig. 1), a number of which contain high-pressure metamorphic rocks (e.g. Windley et al. *1990*; Xiao et al. *1992*, *2004*; Allen et al. *1993*; Ma et al. *1993*; Gao et al. *1995*; Zhou et al. *2001*). The Central Tianshan domain consist of a Proterozoic basement covered by Ordovician-Silurian arc-volcanics, Silurian flysch and subduction-related Silurian-Early Devonian plutons. This substratum is overlain with angular unconformity by Early Carboniferous clastic series that are devoid of calc-alkaline volcanic intercalations (Charvet et al. *2007*; Wang et al. *2008b*, *c*). The South Tianshan domain essentially comprises klippes of ophiolitic mélanges (Fig. 1) constituted by a Late Devonian to Early Carboniferous matrix with blocks of Early Palaeozoic mafic-ultramafic rocks (Charvet et al. *2007*; Wang et al. *2008b*, *c*). Chert from the Wupatarkan Group, which seems to be associated with the westernmost outcrop of the domain near Aheqi (Fig. 1), has yielded Late Permian radiolarians, in addition to Silurian to earliest Carboniferous species (Li et al. *2005a*, *2005b*). The Yili block is located between the Permian Qingbulak-Nalati and North Tianshan strike-slip faults (QNF and NTF; Fig. 1) and described in more detail below.

Tectonism and magmatism

The Palaeozoic Chinese Tianshan evolved from a number of distinct accretion and collision phases involving various microcontinental fragments and magmatic arcs between the Kazakh and Junggar composite continents and the Tarim craton (Windley et al. *1990*; Shi et al. *1994*; Brookfield *2000*; Shu et al. *2000*, *2002*; Zhou et al. *2001*; Xiao et al. *2004*; Buckman and Aitchison *2004*; Wang et al. *2006*, *2007a*, *b*, *2008b*, *c*). Charvet et al. (*2007*) argued that this evolution started in the Late Devonian and ended in the Early(?)-Middle Permian, around 270–260 Ma, using Gradstein et al. (*2004*). Late Permian red beds (Fig. 1) with locally intercalated subaerial volcanic rocks overlie deformed, older Palaeozoic rocks with a regional unconformity in the Tianshan, but also in the northern margin of Tarim (XBGMR *1993*; Allen et al. *1995*; Carroll et al. *1995*, *2001*; Wang et al. *2008a*, this issue). As these terrestrial

sediments overlie Carboniferous marine sedimentary and volcanic series, a major change in palaeogeography and tectonic regime seems to have occurred (Wang et al. *2008a*, this issue).

Bimodal magmatic and volcanic rocks with an alkaline signature of mainly Permian age are widespread throughout the Chinese Tianshan (Allen et al. *1993*; Chen et al. *2000*; Hu et al. *2000*; Mao et al. *2005*; Gao et al. *2006*; Zhou et al. *2006*; Charvet et al. *2007*; Wang et al. *2008a*, this issue). The intrusive rocks are quartz diorite, quartz syenite, granodiorite, monzonite, and K-feldspar granite plutons, as well as abundant dykes (Mao et al. *2005*). Many of them are located along strike-slip faults (Fig. 1). Isotopic ages of various intrusive rocks fall in the 298–252 Ma range (see overviews by Charvet et al. *2007*; Wang et al. *2008a*, this issue). Some of the Permian K-granite dykes are boudinaged or folded, other K-granites have a well-developed mylonitic foliation, illustrating their synkinematic nature (Wang et al. *2008a*, this issue). However, these intrusive rocks cut tectonic foliations related earlier (i.e. late Carboniferous) ductile thrusting (Fig. 2; Wang et al. *2008a*, this issue). This illustrates that the Permian magmatism may be regarded as having occurred after certain block collisions, but definitely not as post-tectonic. Different types of porphyries with 248–278 Ma isotopic ages and many geochemical features of high-SiO_2 adakite intrude basic to acid volcano-sedimentary series as young as middle-late Permian of the central Yili block, to the south of Nileke (Fig. 1) and in the Sanchakou area farther East (Zhao et al. *2007*).

Some large alkali-granite and syenite batholiths were accompanied by alkaline mafic-ultramafic intrusions (Coleman *1989*; Chen and Jahn *2004*; Chen and Arakawa *2005*; Pirajno et al. *2008*; Xiao et al. *2008a*, *b*). These intrusions are composed of peridotite, pyroxenite, troctolite, hornblendite, (alkaline) gabbro and diorite; they typically are funnel-shaped and concentrically zoned, and often occur as elongated outcrops along major fault zones (Chai et al. *2008*; Mao et al. *2008*; Pirajno et al. *2008*; Zhang et al. *2008b*). They have been referred to as Alaskan-type by Xiao et al. (*2008a*, *b*), which occur in linear zones along the trend of major orogenic belts or in convergent margin settings. SHRIMP U–Pb dating of zircon from a number of mineralised intrusions yielded ages of 285–270 Ma, implying that the mafic-ultramafic complexes in Xinjiang also formed in the Early Permian (Zhou et al. *2004*; Zhang et al. *2008a*, *b*, and references therein).

The mafic-ultramafic suites and the basic dyke swarms that commonly accompany them are generally fractionated, implying that they were feeders of flood basalts (Mao et al. *2008*). These swarms comprise diabase, diabase porphyry, diorite and quartz diorite porphyry with K–Ar and Rb–Sr ages of 241–271 Ma (compilation in: Zhao et al. *2008*). Late Carboniferous to Early Permian turbidites are also intruded by these dyke swarms (Allen et al. *1995*; Zhao et al. *2008*). Early Permian rhyolites and tholeiitic to alkaline basalts occur in the Chinese Tianshan (Jiang et al. *2004*). Similar bimodal volcanic series, mafic dykes, ultramafic rocks and syenites crop out in Tarim (Carroll et al. *2001*; Pirajno et al. *2008*). Late Permian alkaline plateau basalts associated with trachyrhyolites and accompanied by intrusions of alkaline granites and gabbro-dolerite dykes (Bakanas complex) and late Permian–earliest Triassic subalkalic basalts, trachytes, ignimbrites, monzonites, syenites (Semeitau complex) prominently feature in eastern Kazakhstan (Allen et al. *1995*). These volcanites measure up to 2 km and cover folded older Palaeozoic rocks (Yakubchuk et al. *2002*). Sanidine crystals from two extrusive units in the Semeitau complex yielded $^{40}Ar/^{39}Ar$ ages of 248.2 ± 0.5 and 248.8 ± 0.5 Ma (Lyons et al. *2002*). Alkaline complexes and carbonatites of Permian to Triassic age were also formed (Konopelko et al. *2007*).

Basaltic underplating

Zhou et al. (*2004*) and Pirajno et al. (*2008*) argued that the coeval and spatially related, voluminous Permian alkaline and peralkaline granitic magmatism on the one hand, and the mafic–ultramafic intrusions and associated Cu–Ni–platinum group element (PGE) sulphide deposits on the other, were due to a common event in the mantle. The Permian alkaline and peralkaline granites are petrogenetically of the A-type (Coleman *1989*) that is formed by a number of processes in the lower crust in non-orogenic, extensional environments, both within-plate and during the waning stages of subduction-zone-related magmatism (Eby *1990*). Anorogenic A-type felsic to intermediate magmatism of alkaline affinity is commonly linked with a variety of ore deposits (Pirajno et al. *2008*, and references therein). The low initial $^{87}Sr/^{86}Sr$ ratios, positive $\varepsilon_{Nd}(t)$ (i.e. the relative deviation of $^{143}Nd/^{144}Nd$ from the chondritic ratio at time *t*) and Sm–Nd (Dm) model ages of 300–1,300 Ma of the A-type granites indicate their largely juvenile character (<40% crustal component) and relatively young extraction from the mantle (Chen et al. *2000*; Heinhorst et al. *2000*; Jahn *2004*; Berzina and Sotnikov *2007*). Chen and Jahn (*2004*) pointed out that such a widespread and important magmatism needs the bottom of the crust to be maintained at a very high temperature (i.e. about 950°C needed for amphibole dehydration melting), with continued influx of basaltic magma (underplating) being a likely mechanism. Massive underplating of basaltic magma at the base of the crust would supply the heat necessary to cause partial melting of its lower part and account for generation of juvenile melts that intruded higher-crustal levels (Chen et al. *2000*; Wu et al. *2002*; Chen and Jahn *2004*; Jahn *2004*; Zhou et al. *2004*; Konopelko et al. *2007*; Chai et al. *2008*; Pirajno et al. *2008*). The parental magmas for the Huangshan layered mafic-ultramafic intrusions (eastern Tianshan) were likely high-Mg tholeiitic basaltic magmas, which too require very high mantle temperatures (Zhou et al. *2004*). Using Sr–Nd–Pb isotope systematics and main and trace element geochemistry Zhao et al. (*2008*) demonstrated that the Permian adakites from the central Yili block originated from partial melting of rutile-bearing amphibole eclogite-facies material at about 45–50 km depth by underplated basaltic magma derived from weakly depleted mantle. Mafic granulite xenoliths occur in basalts intercalated with Cretaceous–Palaeogene red beds of the Tuoyun basin developed on the deformed late Palaeozoic rocks to the north of Tarim (just to the West of Fig. 1) (Zheng et al. *2005*). The authors interpreted a concordant $^{206}Pb/^{238}U$ versus $^{207}Pb/^{235}U$ age of 253 ± 3 Ma for zircons from the xenoliths as constraining the age of metamorphic recrystallisation at a depth of ca. 45 km of mantle-derived basaltic magma that was underplated at the crust-mantle boundary.

Mineralisations: timing and formation mechanisms

Fe, Fe–Cu, and Pb–Zn–Ag deposits related to granite activity, shear zone-hosted gold deposits, and epithermal gold mineralisations were formed between 290 and 240 Ma (Han and Zhao *2003*; Mao et al. *2004a*, *b*, *2005*, *2008*; Yakubchuk *2004*; Han et al. *2006*). Gold mineralisation peaked in the Early Permian, that is 290–270 Ma, related to regional-scale, convective fluid circulation associated to granite intrusions and controlled by transcrustal strike-slip shear zones (Rui et al. *2002*; Han and Zhao *2003*; Zhang et al. *2003*; Mao et al. *2004b*, *2005*; Zhang et al. *2008a*). Part of the mineralisation occurred in the Palaeozoic sedimentary series of the Central Tianshan domain, including in partly volcanic series of Late Carboniferous to Late Permian age (Zhang et al. *2003*; Yang et al. *2006*; Liu et al. *2007*). Some mafic-ultramafic intrusions host orthomagmatic Cu–Ni–(PGE) sulphide deposits (Chai et al. *2008*; Pirajno et al. *2008*; Zhang et al. *2008a*, b). Re–Os dating of such ores from various deposits yielded isochron ages of 298–282 Ma (Mao et al. *2008*). Mafic-ultramafic complexes hosting Cu–Ni–(PGE) deposits are usually affected by locally fracture-controlled

hydrothermal alteration (Mao et al. *2008*; Pirajno et al. *2008*). This process is locally pervasive and resulted in talc-carbonate, biotite–chlorite, sericite–muscovite–chlorite, actinolite–tremolite assemblages (Mao et al. *2008*; Pirajno et al. *2008*).

Alkaline magmatic activity in the Tianshan seems to have come to a halt during the Early Triassic (Allen et al. *1995*). However, mineralisations continued into the Late Triassic (Zhang et al. *2008a*), including shear zone hosted gold deposits with $^{40}Ar/^{39}Ar$ ages of 220.6 ± 0.6 to 222.5 ± 1.2 Ma (Zhu et al. *2006*), and of 208.3 ± 0.6 to 210.6 ± 1.0 Ma (Liu et al. *2007*). At Muruntau in Uzbekistan mineralisation similarly continued into the Triassic, at least 30 Ma later than subjacent felsic intrusions, as indicated by 245 and 220 Ma $^{40}Ar/^{39}Ar$ ages of hydrothermal sericite from selvages to auriferous quartz veins (Wilde et al. *2001*). Graupner et al. (*2005*) interpreted these dates to reflect the age of precipitation of late, Ag-rich gold at temperatures of 230–330°C, during deformation. On the basis of high initial $^{87}Sr/^{86}Sr$ ratios and stable isotope geochemistry of Late Triassic gold deposits in China, Zhu et al. (*2006*) and Liu et al. (*2007*) underscored that although these were shear zone hosted, the ore-forming fluids were unrelated to any magmatic process and derived predominantly from meteoric water of 110–220°C.

The Yili arc: its southern margin and the overthusting high-pressure metamorphics

Calc-alkaline plutonic rocks of the Yili arc have been formed in a continental margin arc and yielded zircon U–Pb ages ranging between 360 and 310 Ma (Li et al. *1998*; Zhu et al. *2006*; Wang et al. *2006*, *2007b*, *2008a*, this issue). Late Carboniferous adakites, derived from partial melting of a subducted slab, occur on different locations (Zhao et al. *2008*; Wang et al. *2008a*, this issue). Carboniferous sediments are intimately associated with large volumes of volcanic rocks (Fig. 1; Wang et al. *2008a*, this issue). Similar-aged series of the Bogda arc s.l., situated in the North Tianshan domain along the southern margin of the Junggar basin (Fig. 1), are regarded as the eastern extension of the Yili arc (Charvet et al. *2007*; Wang et al. *2008c*). Palaeomagnetic data imply that since Late Carboniferous time no significant relative motion occurred between Yili and western part of the Junggar block (Wang et al. *2007a*). The Yili-North Tianshan plutono-volcanic series can be regarded as the easternmost continuation of similar-aged arc rocks in central Kazakhstan. They form a curve-shaped active continental margin arc (Kazakh-Mongol arc: Yakubchuk *2004*, or Balkhash-Yili arc: Filippova et al. *2001*; Windley et al. *2007*) that occurs obliquely superimposed on the regional structure of the Kazakhstan composite continent. The Carboniferous volcano-sedimentary series and older rocks are locally overlain by Permian red, continental clastic rocks and post-collisional volcanites (Wang et al. *2008a*, this issue; Fig. 1).

The Proterozoic crystalline basement of the Yili arc (Hu et al. *2000*) crops out along its margins (Zhou et al. *2001*; Wang et al. *2006*, *2008b*, c). Along the Kekesu River the basement comprises ductilely deformed, steeply dipping granitoids, gabbros, gneisses and (ultra) mylonites (Fig. 2). Southward of this zone a series of biotite–muscovite schist, micaceous quartzite and biotite gneiss is interpreted as the pre-Carboniferous, metamorphosed and deformed sedimentary cover of the Yili arc's Proterozoic basement (Wang *2006*; Wang et al. *2008b*, *c*). Subvertical bodies and sills of Permian granites intrude close to this basement-cover contact, cut the steep ductile foliation, and also intrude parallel to splays of the dextral Qingbulak-Nalati strike-slip fault (Fig. 2), which occurs near the arc's southern margin (QNF, Fig. 1). Such alkaline K-granites along the fault yielded zircons with 280–266 Ma U–Pb ages

(Gao et al. *2006*; Wang et al. *2008a*, this issue). Carboniferous plutonic rocks are cut by the fault (Fig. 2), and strongly mylonitised adjacent to it (Wang et al. *2008c*).

On the basis of Cambrian–Ordovician SHRIMP U–Pb ages obtained on zircons from MORB-type basalts and diorites, Qian et al. (*2008*) regarded the zone of mylonites, gneisses and ductilely deformed granitoids and gabbros of the southernmost part of the basement of the Yili arc as an early Palaeozoic suture zone. They considered the rocks to the south of this suture, which continues westward into the Nikolaev Tectonic Line in Kyrgyzstan, as an independent plate. However, we do not follow this subdivision, as an extensive review by de Jong et al. (*2006*) revealed that many micro-continents in Central and East Asia were rimmed by early Palaeozoic subduction-accretion complexes, island arcs or contained calc-alkaline volcanic margins that were probably formed in the East Gondwanan margin before the building of the Eurasian continent in pre-Early Devonian time.

This southernmost part of the Yili arc's basement has been overthrust by high-pressure metamorphic rocks of the Changawuzi-Kekesu belt (Fig. 1) that forms a suture zone (Wang et al. *2008b*, *c*). The belt principally comprises eclogite–blueschist- and greenschist-facies, in part metagraywacke-like, metasediments that contain numerous lenses and blocks of ultramafic rocks, marbles and eclogites with blueschist layers (Gao et al. *1995*; Gao and Klemd *2003*; Wei et al. *2003*; Klemd et al. *2005*; Lin and Enami *2006*). The Changawuzi-Kekesu belt continues westward to Kyrgyzstan (Atbashy belt: Tagiri et al. *1995*; Stupakov et al. *2004*) and to Tajikistan (Fan-Karategin blueschist belt: Volkova and Budanov *1999*).

The high-pressure metamorphism in the Changawuzi-Kekesu belt is often regarded to have occurred during subduction and accretion in Early Carboniferous time, on the basis of isotopic ages of 345–350 Ma (Xiao et al. *1992*; Gao et al. *1995*; Gao and Klemd *2003*). White mica with varying phengite and paragonite components from partially retrogressed high-pressure metamorphic rocks characterised by abundant late-stage chlorite and albite growth yielded isotopic ages that are upto 50 Ma younger than the age generally attributed to the high-pressure metamorphism (Gao and Klemd *2003*; Klemd et al. *2005*; Wang et al. *2008c*). Klemd et al. (*2005*) interpreted their ca. 300–315 Ma $^{40}Ar/^{39}Ar$ and Rb–Sr ages by a varying degree of greenschist-facies overprint during the tectonic transport of the high-pressure metamorphic rocks to higher level in the crust. Wang et al. (*2008c*) interpreted saddle-shaped age spectra by protracted retrograde (re)crystallisation of the blueschist-facies mineral assemblage during exhumation and thrusting. On the basis of a ca. 316 Ma Ar/Ar plateau age (Fig. 2), Wang et al. (*2008c*) regarded the northward thrusting of the Changawuzi-Kekesu belt over the metasedimentary cover of the crystalline basement of the southern margin of the Yili arc as a Late Carboniferous event that give rise to ductile deformation under greenschist-facies conditions.

$^{40}Ar/^{39}Ar$ Geochronology

We sampled micaceous quartzites and undeformed granite from the southern margin of the Yili arc in which a Permian strike-slip fault is developed, and mylonitic slates from Permian strike-slip fault zones located between the Yili block and the North Tianshan domain (Figs. 1, 2).

Experimental procedures

Single grains of biotite, K white mica and whole-rock fragments were carefully handpicked under a binocular zoom microscope from 0.3 to 2.0 mm size fraction of crushed rock. Following thorough ultrasonic rinsing in distilled water the samples were wrapped in Al foil envelopes (11 mm × 11 mm × 0.5 mm), which were stacked in an irradiation can, with flux monitors inserted after every eight to ten samples. Standard Sanidine TCR-2 [with an age of 28.34 Ma (Renne et al. *1998*)] was used as flux monitor. Samples and standards were irradiated for 13.33 hours at the McMaster reactor (Hamilton, Canada) with a total flux of 1.7×10^{18} n cm^{-2}. The sample arrangement allowed the flux gradient to be monitored with a precision of ±0.2%. Minerals or whole-rock fragments were step-heated with an $^{40}Ar/^{39}Ar$ laser probe (CO_2 Synrad®) at Geosciences Rennes, following the procedure outlined by Ruffet et al. (*1991*, *1995*). Blanks were performed routinely at the start of an experiment and repeated typically after each third run, and subtracted from the subsequent sample gas fractions. Analyses were performed on a MAP215® mass spectrometer.

Plateau ages were calculated if 70% or more of the $^{39}Ar_K$ was released in at least three or more contiguous steps, the apparent ages of which agreeing to within 1σ of the integrated age of the plateau segment.

The $^{40}Ar/^{39}Ar$ analytical data are listed in Table 1, and portrayed as age spectra in Figs. 3 and 4. All errors are quoted at the 1σ level.

Data obtained with a defocussed laser; fusion for the final step is achieved by beam focusing. $^{40}Ar^*$ is radiogenic argon from natural K-decay; $^{40}Ar_{atm}$ is atmospheric ^{40}Ar; $^{37}Ar_{Ca}$, and $^{39}Ar_K$ are Ca- and K-derived Ar during irradiation; *J* irradiation parameter. Decay constant and isotopic abundance ratios used: $^{40}K_{tot} = 5.543 \times 10^{-10}$ a^{-1}; $^{40}K/K = 0.01167$ atom % (Steiger and Jäger *1977*)

Strike-slip faults south of the North Tianshan domain

Sample description

Slates XJ628-7 and XJ703 (Fig. 1; numbered stars 1 and 2, respectively) have been collected from the North Tianshan Fault (Allen et al. *1993*; Zhou et al. *2001*) and its southeastern continuation, the Main Tianshan Shear Zone (Shu et al. *1999*, *2002*; Laurent-Charvet et al. *2003*), respectively, which cross cut the southern margin of the North Tianshan domain (Fig. 1). These ductile shear zones have a steeply dipping foliation that contains a pronounced subhorizontal mineral and stretching lineation. The asymmetry of fabric elements, like, for example shear bands, micro boudins and pressure shadows, indicate dextral shearing. These dark grey, intensely foliated and lineated rocks have quartz, muscovite, biotite, chlorite and plagioclase as main minerals. Their grain-size is too small for a successful mineral separation; hence, we isotopically dated whole-rock fragments instead.

Results and interpretation

Both whole-rock samples yielded irregular, strongly (XJ628-7) or slightly (XJ703) asymmetric dome-shaped age spectra (Fig. 3a, b). The apparent ages for about 90% of the entire gas release are between 255 and 285 Ma (XJ628-7) and between 263 and 275 Ma (XJ703). For both samples, the age spectra are inversely correlated to the U-shaped

$^{37}Ar_{Ca}/^{39}Ar_K$ ratios spectra (Fig. 3a, b). This indicates that the whole-rock samples are chemically heterogeneous and contain different components. The high $^{37}Ar_{Ca}/^{39}Ar_K$ ratios that correspond to the young ages of the first steps probably correspond to carbonate formed during alteration, but part is probably related to chlorite too. The high $^{37}Ar_{Ca}/^{39}Ar_K$ ratios for the steps making up the last 30% of gas release also point to the degassing of a Ca-rich component, which probably is feldspar. The middle part of the spectra has the lowest $^{37}Ar_{Ca}/^{39}Ar_K$ ratios that correspond to the degassing of the most K-rich component mica. The apparent ages of the middle part of the degassing dominated by mica, and the final 30% of the gas release dominated by probably feldspar are comparable. This indicates the thorough dynamic recrystallisation of specifically the feldspar - in all likelihood a detrital component derived from older crystalline rocks.

Yili magmatic arc

Sample description

Plutons of coarse grained, Carboniferous granodiorite, tonalite and granite with K-feldspar megacrysts, pegmatite and aplite dykes of the Yili arc are well developed in the northernmost part of the Kekesu section. Sample XJ620 (Fig. 1; numbered star 3) is a biotite granite taken from a huge pluton. It is an unfoliated, strain-free magmatic rock sampled at about 5 km across strike from the Qingbulak-Nalati strike-slip fault but within the 15–20 km wide zone with steeply dipping tectonic fabrics that are truncated by Carboniferous plutons. Biotite occurs as equidimensional grains, about 500 μm in length. Laser ablation of 120 zircon grains from this sample and applying Inductively Coupled Plasma Mass Spectrometry (LA-ICPMS) yielded a $^{238}U/^{206}Pb$–$^{207}Pb/^{206}Pb$ Concordia age of 313 ± 4 Ma (95% conf. MSWD = 1.02); the ages being distributed symmetrically with a sharp single peak on a cumulative Gaussian probability curve (Wang *2006*, pp. 131–132).

Results and interpretation

Biotite XJ620 yielded a plateau age of 263.4 ± 0.6 Ma over almost the entire gas release (Fig. 4a). Nevertheless the slight hump-shape of the $^{40}Ar/^{39}Ar$ age spectrum suggests a possible minor $^{39}Ar_K$ recoil from the K-rich biotite into K-poor alteration phases during neutron irradiation, such as submicroscopic chlorite, which is quite common for biotite (e.g. Hess and Lippolt *1986*; Ruffet et al. *1991*).

Pre-Carboniferous metasediments basement Yili arc

Along the Kekesu River we sampled two micaceous quartzites from the pre-Carboniferous metasedimentary cover of the steeply dipping Proterozoic basement of the southern margin of the Yili arc (Fig. 2). Samples XJ679 and XJ680 were taken at less than 2 km from an over 20 km long granite sill (Fig. 2). Concordant zircons from this massive pink K-granite yielded an LA-ICPMS weighted mean U–Pb age of 277 ± 3 Ma (Wang et al. *2008a*, this issue). In some mica-rich zones in metapelites from this zone, microscopic sense-of-shear criteria pointing to top-to-the-south shear have been observed, which is in a direction opposite to the overall northward kinematics (Wang *2006*; Wang et al. *2008b*, *c*). This might represent a phase of extensional shearing restricted to mica-rich domains (Wang *2006*).

Sample description

Both samples are lineated and foliated quartzites rich in muscovite (XJ679) or biotite (XJ680). The main minerals quartz and mica form strain-free, equigranular aggregates with straight grain boundaries. Quartz grains are generally equant with their size depending on the amount of mica of layers, but generally remaining below 300 μm. Mica in the quartz matrix of both samples occurs as <100 μm long crystals. Monomineralic, asymmetric, sigmoidal mica aggregates are well over 2,500 μm in length and composed of strain-free crystals that are at least 500 μm long and form a decussate structure with low-rational impingement boundaries.

Results and interpretation

Muscovite XJ679 and biotite XJ680 both yielded concordant plateau ages of 253.3 ± 0.3 and 252.3 ± 0.3 Ma, respectively, over virtually the entire gas release (Fig. 4b). The age concordance indicates that biotite is not affected by incorporation of excess argon, to which the mineral is prone. The regularity and flat nature of the age spectrum indicated that $^{39}Ar_K$ recoil from the K-rich biotite into K-poor alteration phases, such as submicroscopic chlorite, did not occur. This underlines the purity of the used biotite grain. The subtle saddle shape of the age spectrum of muscovite XJ679 suggests minor chemical heterogeneities at the grain scale, which may point to partial recrystallisation or new growth of mica, as will be further discussed below.

Meaning of Permian $^{40}Ar/^{39}Ar$ ages

Mylonitised slates from the North Tianshan Fault (XJ628-7) and its southeastern continuation, the Main Tianshan Shear Zone (XJ703) (Fig. 1) yielded $^{40}Ar/^{39}Ar$ whole-rock age spectra with apparent ages between 255 and 285 Ma and between 263 and 275 Ma, respectively, over almost the entire gas release (Fig. 3). Despite the spectra's dome-shapes, we regard the ages as geologically meaningful and dating the major dextral ductile strike-slip deformation as Middle Permian. These ages are comparable to 240–290 Ma $^{40}Ar/^{39}Ar$ mineral dates from the Main Tianshan Shear Zone and related strike slip zones in Xinjiang obtained by Cai et al. (*1996*), Zhou et al. (*2001*) and Laurent-Charvet et al. (*2003*).

Biotite XJ620 yielded a 263.4 ± 0.6 Ma $^{40}Ar/^{39}Ar$ plateau age (Fig. 4a), which is much younger than the 313 Ma U–Pb age obtained on zircon from this granite that dates the intrusion. The age difference of about 80 Ma is probably too large to be explained by slow cooling of the Yili arc. Although granite XJ602 has intruded into a 15–20 km wide zone of steeply dipping ductile foliations, it lacks deformation fabrics that may be related to the tectonic imprint of the nearby Qingbulak-Nalati strike-slip fault. Consequently, the Middle Permian age of the biotite can not be due to dynamic recrystallisation in the fault zone.

Two micaceous quartzites from the pre-Carboniferous metasedimentary cover of the Yili arc's Proterozoic basement yielded concordant plateau ages of 253.3 ± 0.3 Ma (white mica XJ679) and of 252.3 ± 0.3 Ma (biotite XJ680) (Fig. 4b). The Qingbulak-Nalati strike-slip fault occurs at about 8 km across strike from the site sampled (Fig. 2). In contrast to the ductilely deformed rocks located closer to this fault and that have weakly plunging stretching lineations, the sampled metasediments have steeply plunging lineations (Fig. 2). Consequently, these rocks too do not seem to have been affected by ductile deformation and dynamic recrystallisation related to the strike-slip fault, the movement of which is dated by

synkinematic 277 Ma-old granites (Wang et al. *2008a*, this issue). Cheilletz et al. (*1999*) and Alexandrov et al. (*2002*) have pointed out that saddle-shaped age spectra, similar to the one obtained for muscovite XJ679, may result from the presence of different reservoirs in partially recrystallised mica grains with distinct argon compositions that degas over a different energy interval: a primary, unrecrystallised or inherited domain (low and high temperature steps) and a newly formed or recrystallised one (saddle minimum in the intermediate to high temperature steps). As suggested by Castonguay et al. (*2007*), the younger subdomains formed by growth or recrystallisation could characterise the last isotopic record during a protracted (re)crystallisation history. For muscovite XJ679, this prolonged recrystallisation would have lasted at least 3.5 Ma, between ca. 256 Ma (low and high temperature apparent ages), or slightly older, and ca. 252.5 Ma (saddle minimum). It is striking that this minimum age is perfectly concordant with the plateau age of biotite XJ680 (Fig. 4b). The two concordant ca. 252 Ma plateau ages are probably not due to the thermal influence of the over 20 km long sill of 277 Ma-old granite that occurs less than 2 km across strike, given the age difference of around 25 Ma. As the granite intruded a splay of the Permian Qingbulak-Nalati strike-slip fault and used the basement-cover contact (Fig. 2), the young mica ages thus seem to be best explained by fluid flow in such steep zones after the intrusion was completed. This situation resembles that of the Triassic auriferous quartz veins at Muruntau (Uzbekistan) that contain hydrothermal sericite with $^{40}Ar/^{39}Ar$ ages that are at least 30 Ma younger than neighbouring felsic intrusions (Wilde et al. *2001*). The influence of recrystallisation associated with late-stage ductile extensional deformation localised in metapelites from the zone were XJ679 and XJ680 were sampled is unclear. 330–315 Ma $^{40}Ar/^{39}Ar$ plateau ages of white mica single grains from the same series of pre-Carboniferous metasediments of the Yili arc about 9 km to the South, and from the overlying partially retrogressed blueschists (Wang et al. *2008c*), farther southward (Fig. 2), show that such recrystallisation around the Permian-Triassic boundary did not affect rocks at greater distance from such steeply dipping discontinuities. This fluid-mediated recrystallisation interpretation is extended to the ca. 263 Ma plateau age of biotite from granite XJ620.

Micaschists like those associated with the Kule and Changawuzi ophiolites (Fig. 1), not obviously affected by deformation related to Permian strike-slip faults yielded young $^{40}Ar/^{39}Ar$ ages on biotite (259 ± 3 Ma: Cai et al. (*1996*); 245.0 ± 0.3 Ma: Hao and Liu (*1993*). In the following sections we aim to further explore the possibility that fluid flow, which may be associated with magmatism, is the rationale behind the finding of Permian and younger isotopic ages.

Permian ages: structurally controlled fluid-mediated recrystallisation

Many authors (Rui et al. *2002*; Han and Zhao *2003*; Zhang et al. *2003*; Mao et al. *2004b*, *2005*) showed that the East Tianshan's skarns and gold deposits are associated with emplacement of magmas in Early Permian time (i.e. 290–270 Ma), following an important phase of continental collision. Strontium and stable isotope geochemistry implies that a variety of medium temperature range (180–340°C) fluids were involved in the ore-forming processes, but that late-stage mineralisations appear to have occurred mainly by meteoric water (Zhang et al. *2003*; Yang et al. *2006*). In a study of the late Palaeozoic (ca. 275 Ma) Muruntau gold deposit in western Uzbekistan Graupner et al. (*2006*) also showed that significant amounts of low-temperature meteoric fluids circulated during late-stage mineralisation. Using noble gas, carbon isotope and halogen data, these authors demonstrated a high proportion of crustal components in the main stage mineralising fluids, which they explained by intense fluid–rock interaction in fracture systems that host the deposit.

Sibson (*2007*) pointed out that flow of substantial fluid volumes can be focussed into regions of stress heterogeneity, like shear zone intersections and other fault irregularities (fault tips, jogs, bends, stepovers or offset strands of strike-slip faults, etc.). Also dilatant fault-fracture meshes can function as localised high-permeability conduits, as they form networks of interlinked minor faults and fractures that occupy a substantial volume of the rock-mass. Furthermore, hydrothermal fluids can be drawn into areas where existing fault sets are strongly misoriented, e.g. through inheritance (Sibson *2007*). In strike-slip fault zones, such areas form vertical pipe-like conduits for enhanced fluid flow; magmatic-hydrothermal systems and mineralisations occur in opened fractures in the strongest deformed and thus most permeable rock volume (Sibson *1987*). In this respect it is interesting to note that biotite from gold-bearing mylonitic rocks from the Main Tianshan Shear Zone at Konggur in the East Tianshan yielded an $^{40}Ar/^{39}Ar$ age of 250 ± 8 Ma (Shu et al. *2000*). Yakubchuk et al. (*2002*) noted that most mineral deposits in the Tianshan are related to second- and third-order structures in shear zones that are associated with regional-scale faults. In such shear zones that are undergoing overall ductile deformation, dilation is achieved by interaction of brittle shears. Walther (*1994*) and Zack and John (*2007*) underlined the ability of fluids to hydrofracture rocks during their passage and build interconnected pathways, hence, further intensifying fluid–rock interaction.

As interaction of a circulating fluid with earlier mineralisation and other source rocks seems paramount for their enrichment between the sites of fluid generation and ore deposition (Yakubchuk et al. *2002*), not all fluids become mineralising. The rocks that yielded Permian ages, although not affected by mineralisation, were located in or very close to crustal-scale strike-slip fault systems and might hence have been affected by fluid processes. Since the early laboratory experiments at low temperature (≤200°C) and pressure by Gerling and Ovchinnikova (*1962*) and Kulp and Engels (*1963*) it is known that interaction of circulating solutions with the lattice of minerals can produce cation exchange and that this process can affect their age. Studies in a number of metamorphic terrains worldwide have revealed that fluid-assisted recrystallisation, which affects ionic bonds in minerals, plays a prominent role during exchange or loss of radiogenic daughter isotopes and hence in isotope resetting (Andriessen *1991*; Miller et al. *1991*; Kerrich and Ludden *2000*; Jenkin et al. *2001*; de Jong et al. *2001*; Alexandrov et al. *2002*). Such processes partly occur by low-temperature fluid reaction below the normally used closure temperature, at least for the less robust radiogenic isotope systems (Miller et al. *1991*; Kerrich and Ludden *2000*; Jenkin et al. *2001*). de Jong et al. (*2001*) showed that the degree of submicroscopic illitisation of white mica was more profound in rocks with more closely spaced late-stage hydraulic fractures as these were subjected to an intenser fluid-rock interaction. They argued that illitisation of mica was due to the interaction of meteoric fluids with still hot metamorphic rocks. Consequently, the 263–252 Ma $^{40}Ar/^{39}Ar$ ages that we obtained on mica may be related to regional-scale fluid flow associated with alkaline and peralkaline granite intrusions controlled by steeply dipping transcrustal zones.

Prolonged fluid flow: young ages for early HP metamorphism

The picture that emerges is that in the Permian a convective fluid system, driven by magmatic heat, seems to have been active in a strongly fractured and weakened crust with an elevated heat flow. A number of recent isotope studies have revealed that mineralisations in Central Asia continued into the Late Triassic, apparently after the waning of magmatism (Wilde et al. *2001*; Zhu et al. *2006*; Liu et al. *2007*) and mainly deposited by low-temperature meteoric fluids (Zhang et al. *2003*; Yang et al. *2006*). Such a prolonged hydrothermal activity may also

explain the finding of surprisingly young Permian and even Triassic isotopic age estimates for the high-pressure metamorphism, to which generally a geologically meaningful earliest Carboniferous age is assigned.

Stupakov et al. (*2004*) obtained $^{40}Ar/^{39}Ar$ plateau ages of 327–324 Ma on three phengites from the Atbashy eclogite belt in Kyrgyzstan. However, only one out of three glaucophanes from these samples yielded an $^{40}Ar/^{39}Ar$ age concordant to the corresponding phengite age; the other two samples gave ages of 281 ± 11 and 182 ± 5 Ma. It has been discussed elsewhere (Sisson and Onstott *1986*; de Jong et al. *2006* and references therein) that because glaucophane is K-poor, submicroscopic inclusions of K-rich minerals like mica, which may have formed during or affected by later recrystallisation, may critically influence its age. The important age spread in the Atbashy glaucophanes clearly underlines this point. Tagiri et al. (*1995*) published a 267 ± 5 Ma Omp–Grt–Ph–WR, Rb–Sr isochron age for an eclogite from this belt. The $^{87}Sr/^{86}Sr$ ratio of their sample shows that the age information fundamentally refers to phengite, as the $^{87}Sr/^{86}Sr$ ratios of omphacite, garnet and the whole-rock are virtually identical, due to unfavourable enrichment factors of radiogenic ^{87}Sr. Inspection of their isotopic data further reveals that the two phengites in their sample have strongly contrasting $^{87}Sr/^{86}Sr$ and $^{87}Rb/^{86}Sr$ ratios. This points to isotopic disequilibrium and the presence of two generations of white mica in their sample, in all likelihood due to recrystallisation. A recalculation with Isoplot v3.0 (Ludwig *2003*) using both phengite points of Tagiri et al. (*1995*) yielded a meaningless Omp–Grt–Ph–WR age of 31 ± 170 Ma (2σ; input errors: $^{87}Rb/^{86}Sr$ = 1%, $^{87}Sr/^{86}Sr$ = 0.005%). Recalculating the age without the youngest phengite - that is the least enriched in ^{87}Sr - yielded an age of 267 ± 27 Ma (2σ; MSWD = 10.3; same input errors). This critically underscores the fact that if the oldest phengite was affected by only minor recrystallisation the Rb-Sr age of the eclogite would be significantly older than 267 Ma, and be more in line with the Carboniferous $^{40}Ar/^{39}Ar$ phengite ages obtained by Stupakov et al. (*2004*).

Zhang et al. (*2007*) recently obtained 233 ± 4 to 226 ± 5 Ma U–Pb ages using the SHRIMP on rims of zircon from eclogites and metapelites of the Changawuzi-Kekesu complex at Changawuzi (Fig. 1). On the basis of these ages they suggested that the subduction-related metamorphism was not of Carboniferous age. Arguing in favour of a Triassic age for the high-pressure metamorphism, Zhang et al. (*2007*) suggested that excess argon affected many previously published Carboniferous and older $^{40}Ar/^{39}Ar$ ages. Indeed, it is widely acknowledged that strongly restricted fluid mobility is responsible for the very low lattice and grain boundary diffusion under dry, (ultra) high-pressure metamorphic conditions that result in the survival of too old, pre-orogenic, inherited Rb–Sr and K–Ar ages (Ruffet et al. *1995*, *1997*; de Jong *2003*, and references therein). However, we do not regard this mechanism as a plausible interpretation for the case under discussion. In the first place the available concordant isotopic ages for the high-pressure metamorphism in different parts of the Changawuzi-Kekesu complex, obtained by a number of isotope systems do not point to excess argon. This is critically shown by the following data: 351 ± 2 Ma $^{40}Ar/^{39}Ar$ glaucophane age (Xiao et al. *1992*), 346 ± 3 and 344 ± 1 Ma Sm–Nd garnet-glaucophane and $^{40}Ar/^{39}Ar$ crossite ages, respectively (Gao and Klemd *2003*), and a 346 ± 7 Ma $^{40}Ar/^{39}Ar$ phengite plateau age (Gao et al. *1995*). Secondly, in line with our interpretation of the 263–252 Ma $^{40}Ar/^{39}Ar$ mica ages, we would like to hint that these surprisingly young zircon ages are also somehow controlled by recrystallisation during regional-scale fluid flow. Neoformation of zircon has been described from rocks affected by recrystallisation during regional metamorphism of very-low-grade to high-grade (temperature range: ca. 250°C to >650°C; Carson et al. *2002*; Breeding et al. *2004*; Dempster et al. *2004*; Rasmussen *2005*),

contact metamorphism (ca. 500–600°C; Fraser et al. *2004*), hydrothermal alteration (Rubin et al. *1989*, *1993*; Kerrich and King *1993*; Hoskin *1999*) and rodingitisation (i.e. metasomatic enrichment in Ca-silicates) of eclogites (Li et al. *2005a*, *b*). In all these cases newly formed zircon principally occurs as discrete and less than 3 μm overgrowths on older detrital or magmatic grains or in micro-fractures in them. These areas provided a suitable isostructural substrate for precipitation of mobilised Zr, nucleation and fluid-mediated growth of the mineral (Rasmussen *2005*). Growth of hydrothermal zircon occurs in contact metamorphic and metasomatic environments, hydrothermal veins, hydrothermally altered intrusive and extrusive igneous rocks, as well as mineralised shear zones (Rubin et al. *1989*), indicating that Zr can be highly mobile in such systems. Part of the hydrothermal zircon growth is associated with mesothermal gold deposits (Kerrich and King *1993*; Hoskin *1999*). The latter author suggested that F-ligands may have played a role in Zr transportation during hydrothermal W–Au mineralisation. Although mobility of zirconium seems to be the most common in F-rich hydrothermal systems related to alkalic, F-rich igneous suites, it may also have been promoted by sulphate complexing (Rubin et al. *1993*). It is well documented that fluids of ca. 500–675°C can affect the U–Pb isotopic system of zircon by fluid-mediated growth/recrystallisation along sub-micrometre scale (<0.25 μm) near-surface grain boundary areas and micro-fractures, if infiltration acts jointly with other factors, such as pervasive deformation (Carson et al. *2002*; Breeding et al. *2004*). Such processes may have been operative in eclogites enclosed in the ultramafic rocks at Changawuzi. Triggered by a process of secondary serpentinisation, some eclogites were intensely rodingitised at 300 ± 50°C and 0.2–1.0 GPa during their advanced exhumation (Li et al. *2007*). These authors envisaged that Ca released during clinopyroxene breakdown was concentrated in the driving fluid as the element could not be incorporated in minerals making up the serpentine. The age of the rodingitisation is constrained by $^{206}Pb/^{238}U$ single grain ages of about 291 Ma obtained on unzoned zircon crystals (Li et al. *2005a*, *b*). Most zircons in these rocks are distinctly zoned, and jagged micro-fractures that cross crystal rims were interpreted as fluid channels (Li et al. *2005a*, *b*). The authors underscored that continuous fluid alteration lies behind age differences between zircon rims (291 Ma) and cores (422 Ma; formed during hydrothermal sea-floor metamorphism), as well as contrasting REE patterns that they obtained. It must be borne in mind that also the Early Permian mafic-ultramafic complexes hosting Cu–Ni–(PGE) sulphide deposits usually exhibit strong serpentinisation, uralitisation, chloritisation and tremolitisation that are partly fracture-controlled and may be due to convective hydrothermal fluid circulation (Mao et al. *2008*; Pirajno et al. *2008*). Although the rodingitisation is of Early Permian age, the 245.0 ± 0.3 Ma $^{40}Ar/^{39}Ar$ age of a biotite in micaschists enclosed in the Changawuzi ultramafic rocks (Hao and Liu *1993*) suggests that these rocks were affected by early Triassic recrystallisation too. Fluid-assisted recrystallisation and new growth of zircon may thus be feasible mechanisms to explain the Triassic SHRIMP ages in their rims.

Tectonic implications

Xiao et al. (*2008a*, *b*, this issue) envisaged that a number of arcs accreted up to the end-Permian or even Triassic, taking the 233–226 Ma age estimates of Zhang et al. (*2007*) for ultrahigh-pressure metamorphism in the Changawuzi-Kekesu complex at face value. The Early Permian basic lavas, “Alaskan-type” mafic-ultramafic complexes and granitic plutons, as well as their spatial association with arc–accretion complexes in the Tianshan suggest, according to Xiao et al. (*2008a*), that these rocks were generated in a subduction-related setting. Xiao et al. (*2008a*, this issue) suggest that the presence of adakitic rocks may point to flat subduction. We have discussed above that like many mica ages, the Triassic zircon dates might be due to fluid-mediated recrystallisation and new growth and do not refer to the age of

the high-pressure metamorphism. There are also tectonic arguments against a Triassic age for the high-pressure metamorphism and final terrane accretion in the southern part of the Tianshan belt. These zircon ages are much younger than the Late Carboniferous northward thrusting of the Changawuzi-Kekesu complex over the Yili arc's southern margin. Ca. 300–330 Ma isotopic ages in this complex have been attributed to partial retrogression of the high-pressure metamorphic rocks during this event (Klemd et al. *2005*; Wang et al. *2008c*). Moreover, these Triassic SHRIMP ages are younger than the Permian strike-slip deformation that reworked the suture zone that was formed following the subduction-related metamorphism that produced the very eclogites. As pointed out in the Introduction of this paper, amalgamation of different continents like Kazakhstan, Tarim and Siberia seems to have been essentially completed by Permian–Triassic boundary times. Finally, no indications have been found for tectonism of Triassic age that can be associated with neither subduction that generated the ultrahigh-pressure metamorphic rocks nor their exhumation. Regarding the Permian "Alaskan-type" mafic-ultramafic intrusions and the associated Cu–Ni–(PGE) sulphide deposits it has been underscored by a number of authors (Zhou et al. *2004*; Chai et al. *2008*; Pirajno et al. *2008*; Zhang et al. *2008a*, b) that the geochemical signatures and Re–Sr–Nd isotope systematics of a number of them revealed that they were formed by interaction between depleted asthenospheric melts and metasomatised lithospheric mantle, enriched in upper continental crustal components. These authors pointed out that these chemical characteristics do not point to a generation in a Permian arc setting but that these rocks inherited arc-like fingerprints, which their source rocks obtained during subduction before the Early Permian.

The northward thrusting of the Changawuzi-Kekesu complex over the Yili arc's southern margin and the resulting collision with the Central Tianshan domain developed to the south of the high-pressure metamorphic belt took place in the Late Carboniferous. It is interesting to note that the age of this event coincides with the waning stages of calc-alkaline magmatic activity in the Yili arc, suggesting a causal relationship between them. The Permian bimodal magmatic activity is thus post-collisional with respect to the docking of the Central Tianshan domain. The magmatism of the northwestern Chinese Tianshan shows a compositional variation from highly fractionated calc-alkaline (Late Carboniferous) to alkaline (Permian), the transition occurring around the Carboniferous-Permian boundary (Wang et al. *2008a*, this issue). This points according to these authors to the contribution of multiple magma sources during the transition from Carboniferous convergence to the Permian period dominated by strike-slip tectonism. Wang et al. (*2003*) argued that the Late Palaeozoic magmatic and thermal event, which caused the crust to undergo partial melting and differentiation, is the rationale behind their finding of a homogeneous crust with a subhorizontal seismic velocity structure and low Poisson's ratios within the entire upper and middle part, along a refraction profile across the eastern Tianshan and eastern margin of the Tarim basin. The Late Permian unconformity observed in entire Xinjiang (Allen et al. *1995*; Carroll et al. *1995*, *2001*; Wang et al. *2008a*, this issue) might be due to a regional scale thermal doming related to this magmatic activity.

The generation of alkali-rich granites, mafic–ultramafic intrusions, basic dyke swarms and plateau basalts associated with felsic lavas in Permian time has often been regarded as due to lithospheric extension driven by underplating owing to upwelling of asthenospheric mantle in plumes (e.g. Dobretsov *2003*; Zhou et al. *2004*; Kovalenko et al. *2004*; Berzina and Sotnikov *2007*; Tsygankov et al. *2007*; Pirajno et al. *2008*; Zhang et al. *2008a*). However, in recent years the view that deep mantle plumes are responsible for the formation of large volcanic provinces—such as the classic examples of Hawaii and Pacific seamount trails, Iceland and

Yellowstone—has been challenged by amongst others: Humphreys et al. (*2000*), Christiansen (*2001*), Christiansen et al. (*2002*), Foulger (*2002*), Foulger and Natland (*2003*) and Koppers and Staudigel (*2005*). In a review, Christiansen (*2001*) advocated that the Yellowstone and eastern Snake River Plain rhyolite-basalt association of the western United States, with fracture-controlled, mid-Miocene and early Pliocene epithermal gold-silver deposits (John *2001*), was not generated by a mantle plume. Instead, Christiansen (*2001*) argued that its formation was due to the intersection of an oceanic spreading ridge and the continental-margin trench bordering the North America plate. As a result, an earlier mainly andesitic and calc-alkaline volcanic system terminated as subduction in the area of intersection ceased and that segment of the trench closed. From that moment on, this part of the North America plate margin experienced intraplate extension due to the highly oblique interaction with the Pacific plate. Christiansen (*2001*) envisaged that the basaltic magmas represent partial melting of peridotitic upper mantle in a region of extensional pressure release, and that these were able to rise in a deeply penetrating extensional stress field. Hyndman et al. (*2005*) interpreted the broad belt of distributed deformation in the leading edge of the North America plate by its prolonged position in a backarc, rendering the continental lithosphere hot and consequently weak. In the earliest Permian the Tianshan changed from a continental margin arc to a strike-slip tectonic regime with fault-controlled bimodal magmatism volcanism and ore deposits. This evolution might thus similarly be the consequence of interaction of a spreading centre with a trench system that induced dominant strike-slip deformation and localised extension in the weakened lithosphere of this former continental margin arc during continued oblique plate interaction. Subduction of oceanic spreading ridges leading to slab window magmatism (Yakubchuk et al. *2002*; Windley et al. *2007*), and slab break-off induced basaltic underplating (Wu et al. *2002*; Chen and Arakawa *2005*; Chai et al. *2008*), could be of local importance in such a scenario. This scenario is supported by the palaeomagnetic data of Wang et al. (*2007a*) that reveal highly oblique plate interaction during the Late Carboniferous to Late Permian. During this period the single Yili-west Junggar domain moved by a considerable amount (1,160 ± 380 km) to the east relative to Tarim and Siberia that remained stationary with respect to each other. The occurrence of Late Permian radiolarians in chert of an ophiolitic mélange near Aheqi (Fig. 1) has been interpreted by the presence of a Late Permian oceanic basin to the north of Tarim (Li et al. *2005a*, *b*). Xiao et al. (*2008a*) regarded these cherts as the youngest components in a subduction–accretion complex. It might be speculated that the final docking of the Tarim continent with southern margin of the Central Tianshan–Yili-west Junggar domain might have been instrumental for the cessation of this extensional–transtensional tectono-magmatic regime.

The similarity of ages of the Semeitau magmatic complex in eastern Kazakhstan and the Siberian Traps may point to a genetic relationship between the two (Lyons et al. *2002*). Courtillot et al. (*1999*) proposed that the ca. 251 Ma Siberian traps were emplaced during a phase of latest Permian to Early–Middle Triassic rifting that was aborted and did not lead to continental breakup. This may imply that extension around the Permian-Triassic boundary might have affected part of the much stronger cratons too. Consequently, during the entire Permian period much of Central Asia experienced an extensional-transtensional tectonic regime with an elevated heat flow. This created syn-tectonic bimodal magmatism and a strongly fractured crust in which a convective fluid system was maintained, leading to isotope resetting at regional scale.

Conclusion

Collision in the Chinese western Tianshan evolved from overthrusting in Late Carboniferous time to a regional-scale strike-slip regime in the Permian. $^{40}Ar/^{39}Ar$ apparent ages in the range of 255–285 Ma and 263–275 Ma of two mylonitic whole-rock samples constrain the timing of dextral ductile strike-slip deformation along the southern margin of the North Tianshan domain.

From the southern margin of the Yili arc we obtained a 263.4 ± 0.6 Ma plateau age (1σ) on biotite from an undeformed Early Carboniferous granite, and plateau ages of 253.3 ± 0.3 and 252.3 ± 0.3 Ma (1σ) on, respectively, muscovite and biotite from pre-Carboniferous metasediments covering the arc's Proterozoic basement. The samples were taken at about 5 and 2 km, respectively, across strike from the Permian Qingbulak-Nalati strike-slip fault, but are unaffected by strike-slip deformation. However, they are located within the 15–20 km wide zone with steeply dipping tectonic fabrics that is like the Qingbulak-Nalati strike-slip fault used by intruding Permian granite. The youngest micas are about 25 Ma younger than a neighbouring Permian granite. Consequently, we do not interpret the ca. 250–265 Ma mica ages by the direct thermal effect of intruding granite, but by recrystallisation of the mica by fluid flow, which may be late magmatic, channelled into these steep zones. The slight saddle shape of the muscovite age spectrum, indicative of minor chemical heterogeneities of mica due to new growth and/or its partial recrystallisation, agrees with interpretation. Other muscovite from pre-Carboniferous metasediments of the Yili arc that are located farther away from this strike-slip fault system are not affected by this process.

In the Permian the Tianshan was affected by a Yellowstone-like extensional–transtensional tectonic regime with syn-tectonic bimodal magmatism. Gold mineralisation, tracing aqueous flow in the crust, peaked in Permian time and continued locally into the Triassic. In the strongly fractured and weakened crust with an elevated heat flow, convective fluid systems, partly driven by magmatic heat, may have been active, leading to regional-scale isotope resetting. We suggest that surprisingly young isotopic ages for early orogenic eclogites included in ophiolites in some of the Tianshan's suture zones also relate to fluid-mediated recrystallisation processes that occurred well after Late Carboniferous suturing.

Acknowledgments The senior author (KdJ) would like to dedicate this work to the memory of Prof. Oen Ing Soen, his teacher in ore geology at the University of Amsterdam, and his advice to never underestimate the role of fluids. This work was undertaken while KdJ was associated to the Institute of Advanced Studies Studium® (CNRS and Région Centre) on the invitation of Prof. Michel Faure. The analytical work was financed by *l'Institut des Sciences de la Terre d'Orléans* (ISTO). This research is supported by the National Basic Research Program of China (973 Program) (Nos. 2007CB411301 and 2001CB409804). Funding of a part of the research of BW in France by the French Embassy in Beijing and the French-Chinese Advanced Research Program (PRA T05-02) is gratefully acknowledged. Colleagues of the Bureau of National project 305, Xinjiang Uyghur Autonomous Region are thanked for their help with logistic support during fieldwork. The paper benefitted from reviews and suggestions from Jun Gao and Reiner Klemd. The invitation by topic editor Wenjiao Xiao to place our results in a geodynamic context is appreciated. Jun Gao and Wenjiao Xiao are thanked for kindly supplying pre-prints of their work. Nina Volkova supplied some of the Russian literature used.

References

Alexandrov P, Ruffet G, Cheilletz A (2002) Muscovite recrystallization and saddle-shaped $^{40}Ar/^{39}Ar$ age spectra: example from the Blond granite (Massif Central, France). Geochim Cosmochim Acta 66:1793–1807

Allen MB, Şengör AMC, Natal'in BA (1995) Junggar, Turfan and Alakol basins as Late Permian to ? Early Triassic extensional structures in a sinistral shear zone in the Altaid orogenic collage, Central Asia. J Geol Soc Lond 152:327–338

Allen MB, Windley BF, Zhang C (1993) Paleozoic collisional tectonics and magmatism of the Chinese Tien Shan, Central Asia. Tectonophysics 220:89–115

Andriessen PAM (1991) K–Ar and Rb–Sr age determinations on mica of impure marbles of Naxos, Greece: the influence of metamorphic fluids and lithology on the blocking temperature. Schweiz Mineral Petrogr Mitt 71:89–99

Berzina P, Sotnikov VI (2007) Character of formation of the Erdenet-Ovoo porphyry Cu-Mo magmatic center (northern Mongolia) in the zone of influence of a Permo-Triassic plume. Russ Geol Geoph 48:141–156. doi:10.1016/j.rgg.2007.01.001

Breeding CM, Ague JJ, Grove M, Rupke AL (2004) Isotopic and chemical alteration of zircon by metamorphic fluids: U–Pb age depth-profiling of zircon crystals from Barrow's garnet zone, northeast Scotland. Am Min 89:1067–1077

Brookfield ME (2000) Geological development and Phanerozoic crustal accretion in the western segment of the southern Tienshan (Kyrgyzstan, Uzbekistan and Tajikistan). Tectonoph 328:1–14

Buckman S, Aitchison JC (2004) Tectonic evolution of Paleozoic terranes in West Junggar, Xinjing, NW China. In: Malpas J, Fletcher CJN, Ali JR, Aitchison JC (eds) Aspects of the tectonic evolution of China. Geol Soc Lond Spec Publ 226, pp 101–129

Buslov MM, Fujiwara Y, Iwata K, Semakov NN (2004) Late Paleozoic–Early Mesozoic geodynamics of Central Asia. Gond Res 7:791–808

Cai DS, Lu HF, Jia D, Wu SM, Chen CM (1996) $^{40}Ar/^{39}Ar$ dating of the ophiolite mélange in the southern Tien Shan and the mylonite in the southern rim of central Tien Shan and their tectonic significance (in Chinese with English abstract). Sci Geol Sin 31:384–390

Carroll AR, Graham SA, Chang EZ, McKnight C (2001) Sinian through Permian tectonostratigraphic evolution of the northwestern Tarim basin, China. In: Hendrix MS, Davis GA (eds) Paleozoic and Mesosoic tectonic evolution of central Asia: from continental assembly to intracontinental deformation. Geoph Soc Amer Mem, vol 194, pp 47–69

Carroll AR, Graham SA, Hendrix MS, Ying D, Zhou D (1995) Late Paleozoic tectonic amalgamation of NW China: sedimentary records of the northern Tarim, northwestern

Turpan, and southern Junggar basins. Geol Soc Am Bull 107:571–594

Carson CJ, Ague JJ, Grove M, Coath CD, Harrison TM (2002) U–Pb isotopic behaviour of zircon during upper-amphibolite facies fluid infiltration in the Napier Complex, east Antarctica. Earth Planet Sci Lett 199:287–310

Castonguay S, Ruffet G, Tremblay A (2007) Dating polyphase deformation across low-grade metamorphic belts: An example based on $^{40}Ar/^{39}Ar$ muscovite age constraints from the southern Quebec Appalachians, Canada. Geol Soc Am Bull 119:978–992. doi:10.1130/B26046.1

Chai FM, Zhang ZC, Mao JW, Dong LH, Zhang ZH, Wu H (2008) Geology, petrology and geochemistry of the Baishiquan Ni-Cu-bearing mafic-ultramafic intrusions in Xinjiang, NW China: Implications for tectonics and genesis of ores. J Asian Earth Sci 32:218–235. doi:10.1016/j.jseaes.2007.10.014

Charvet J, Shu SL, Laurent-Charvet S (2007) Paleozoic structural and geodynamic evolution of eastern Tianshan (NW China): welding of the Tarim and Junggar plates. Episodes 30:162–186

Cheilletz A, Ruffet G, Marignac C, Kolli O, Gasquet D, Féraud G, Bouillin JP (1999) $^{40}Ar/^{39}Ar$ dating of shear zones in the Variscan basement of Greater Kabylia (Algeria). Evidence of an Eo-Alpine event at 128 Ma (Hauterivian-Barremian boundary): geodynamic consequences. Tectonophysics 306:97–116

Chen B, Arakawa Y (2005) Elemental and Nd–Sr isotopic geochemistry of granitoids from the West Junggar foldbelt (NW China), with implications for Phanerozoic continental growth. Geochim Cosmochim Acta 69:1307–1320

Chen B, Jahn BM (2004) Genesis of post-collisional granitoids and basement nature of the Junggar Terrane, NW China: Nd–Sr isotope and trace element evidence. J Asian Earth Sci 23:691–703

Chen JF, Zhou TX, Xie Z, Zhang X, Guo XS (2000) Formation of positive $\varepsilon_{Nd}(T)$ granitoids from the Alataw Mountains, Xinjiang, China, by mixing and fractional crystallization: implication for Phanerozoic crustal growth. Tectonophysics 328:53–67

Chiaradia M, Konopelko D, Seltmann R, Cliff RA (2006) Lead isotope variations across terrane boundaries of the Tien Shan and Chinese Altay. Mineral Depos 41:411–428

Christiansen RL (2001) The Quaternary and Pliocene Yellowstone Plateau volcanic field of Wyoming, Idaho, and Montana. US Geol Surv Prof Pap 729-G:144

Christiansen RL, Foulger GR, Evans JR (2002) Upper-mantle origin of the Yellowstone hotspot. GSA Bull 114:1245–1256

Cocks LRM, Torsvik TH (2007) Siberia, the wandering northern terrane, and its changing geography through the Palaeozoic. Earth-Sci Rev 82:29–74. doi:10.1016/j.earscirev.2007.02.001

Coleman RG (1989) Continental growth of northwest China. Tectonics 8:621–635

Courtillot V, Jaupart C, Manighetti I, Tapponnier P, Besse J (1999) On causal links between flood basalts and continental breakup. Earth Planet Sci Lett 166:177–195

de Jong K (2003) Very fast exhumation of high-pressure metamorphic rocks with excess ^{40}Ar and inherited ^{87}Sr, Betic Cordilleras, southern Spain. Lithos 70:91–110

de Jong K, Féraud G, Ruffet G, Amouric M, Wijbrans JR (2001) Excess argon incorporation in phengite of the Mulhacén Complex: submicroscopic illitization and fluid ingress during late Miocene extension in the Betic Zone, south-eastern Spain. Chem Geol 178:159–195

de Jong K, Xiao WJ, Windley BF, Masago H, Lo CH (2006) Ordovician ^{40}Ar/^{39}Ar phengite ages from the blueschist-facies Ondor Sum subduction–accretion complex (Inner Mongolia) and implications for the early Paleozoic history of continental blocks in China and adjacent areas. Am J Sci 306:799–845. doi:10.2475/10.2006.02

Dempster TJ, Hay DC, Bluck BJ (2004) Zircon growth in slate. Geology 32:221–224

Dobretsov NL (2003) Evolution of structures of the Urals, Kazakhstan, Tien Shan, and Altai-Sayan region within the Ural-Mongolian Fold Belt (Paleoasian Ocean). Russ Geol Geophys 44:5–27

Eby GN (1990) The A-type granitoids: a review of their occurrence and chemical characteristics and speculations on their petrogenesis. Lithos 26:115–134. doi:10.1016/0024-4937(90)90043-Z

Filippova IB, Bush VA, Didenko AN (2001) Middle Paleozoic subduction belts: the leading factor in the formation of the Central Asian fold-and-thrust belt. Russ J Earth Sci 3:405–426

Foulger GR (2002) Plumes, or plate tectonic processes? Astron Geoph 43:6.19–23

Foulger GR, Natland JH (2003) Is “Hotspot” volcanism a consequence of plate tectonics? Science 300:921–922

Fraser GL, Pattison DRM, Heaman LM (2004) Age of the Ballachulish and Glencoe Igneous Complexes (Scottish Highlands), and paragenesis of zircon, monazite and baddeleyite in the Ballachulish Aureole. J Geol Soc Lond 161:447–462

Gao J, Klemd R (2003) Formation of HP-LT rocks and their tectonic implications in the western Tianshan Orogen, NW China: geochemical and age constraints. Lithos 66:1–22

Gao J, He GQ, Li MS, Xiao XC, Tang YQ (1995) The mineralogy, petrology, metamorphic PTt trajectory and exhumation mechanism of blueschists, south Tianshan, northwestern China. Tectonoph 250:151–168

Gao J, Long LL, Qian Q, Huang DZ, Su W, Klemd R (2006) South Tianshan: a Late Paleozoic or a Triassic orogen? (in Chinese with English abstract). Acta Petrol Sin 22:1049–1061

Gerling EK, Ovchinnikova GV (1962) Causes of low age values determined on micas by the Rb–Sr method (in Russian). Geokhimiya 9:755–762

Gradstein FM, Ogg JG, Smith AG, Bleeker W, Lourens LJ (2004) A new geologic time scale, with special reference to Precambrian and Neogene. Episodes 27:83–100

Graupner T, Kempe U, Klemd R, Schussler U, Spooner ETC, Gotze J, Wolf D (2005) Two stage model for the Muruntau (Uzbekistan) high grade ore structures based on characteristics of gold, host quartz and related fluids. Neues Jahrb Mineral Abhl 181:67–80

Graupner T, Niedermann S, Kempe U, Klemd R, Bechtel A (2006) Input of mantle fluids into the giant Muruntau Au system: noble gas, carbon isotope and halogen geochemistry of ore fluids. Geochim Cosmochim Acta 70:5356–5370

Han CM, Zhao GC (2003) Major types and characteristics of Late Paleozoic ore deposits, East Tianshan, northwest China. Int Geol Rev 45:798–810

Han CM, Xiao WJ, Zhao GC, Mao JW, Yang JM, Wang ZL, Yan Z, Mao QQ (2006) Geological characteristics and genesis of the Tuwu porphyry copper deposit, Hami, Xinjiang, Central Asia. Ore Geol Rev 29:77–94

Hao J, Liu XH (1993) Ophiolite mélange time and tectonic evolutional model in South Tien Shan area (in Chinese with English abstract). Sci Geol Sin 28:93–95

Heinhorst J, Lehmann B, Ermolov P, Serykh V, Zhurutin S (2000) Paleozoic crustal growth and metallogeny of Central Asia: evidence from magmatic-hydrothermal ore systems of Central Kazakhstan. Tectonophysics 328:69–87

Hess JC, Lippolt HJ (1986) Kinetics of Ar isotopes during neutron irradiation: ^{39}Ar loss from minerals as a source or error in ^{40}Ar/^{39}Ar dating. Chem Geol 59:233–236

Hoskin PWO (1999) SIMS determination of μg g-1-level fluorine in geological samples and its concentration in NIST SRM 610. Geostandard Newslett 23:69–76

Hu A, Jahn B-M, Zhang G, Chen Y, Zhang Q (2000) Crustal evolution and Phanerozoic crustal growth in northern Xinjiang: Nd isotopic evidence. Part 1. Isotopic characterization of basement rocks. Tectonoph 328:15–51

Humphreys ED, Dueker KG, Schutt DL, Smith RB (2000) Beneath Yellowstone: evaluating plume and nonplume models using teleseismic images of the upper mantle. GSA Today 10:1–7

Hyndman RD, Currie CA, Mazzotti SP (2005) Subduction zone backarcs, mobile belts, and orogenic heat. GSA Today 15:4–10. doi:10:1130/1052-5173(2005)015<4:SZBMBA>2.0.CO;2

Jahn B-M (2004) The Central Asian Orogenic Belt and growth of the continental crust in the Phanerozoic. In: Malpas J, Fletcher CJN, Ali JR, Aitchison JC (eds) Aspects of the tectonic evolution of China. Geol Soc Lond Spec Publ, vol 226, pp 73–100

Jenkin GRT, Ellam RM, Rogers G, Stuart FM (2001) An investigation of the closure temperature of the biotite Rb–Sr system: the importance of cation exchange. Geochim Cosmochim Acta 65:1141–1160

Jiang C, Zhang P, Lu D, Bai K, Wang Y, Tang S, Wang J, Yang C (2004) Petrology, geochemistry and petrogenesis of the Kalpin Basalts and their Nd, Sr and Pb isotopic compositions (in Chinese with English abstract). Geol Rev 50:492–500

John DA (2001) Miocene and early Pliocene epithermal gold-silver deposits in the northern Great Basin, western United States: characteristics, distribution, and relationship to magmatism. Econ Geol 96:1827–1854

Kerrich R, King R (1993) Hydrothermal zircon and baddeleyite in Val-d'Or Archean mesothermal gold deposits: characteristics, compositions, and fluid-inclusion properties, with implications for timing of primary gold mineralization. Can J Earth Sci 30:2334–2351. doi:10.1139/cjes-30-12-2334

Kerrich R, Ludden J (2000) The role of fluids during formation and evolution of the southern Superior Province lithosphere: an overview. Can J Earth Sci 37:135–164

Klemd R, Bröcker M, Hacker BR, Gao J, Gans P, Wemmer K (2005) New age constraints on the metamorphic evolution of the high-pressure/low-temperature belt in the western Tianshan mountains, NW China. J Geol 113:157–168

Konopelko D, Biske G, Seltmann R, Eklund O, Belyatsky B (2007) Hercynian post-collisional A-type granites of the Kokshaal Range, Southern Tien Shan, Kyrgyzstan. Lithos 97:140–160. doi: 10.1016/j.lithos.2006.12.005

Koppers AAP, Staudigel H (2005) Asynchronous bends in Pacific Seamount Trails: a case for extensional volcanism? Science 307:904–907

Kovalenko VI, Yarmolyuk VV, Kovach VP, Kotov AB, Kozakov IK, Salnikova EB, Larin AM (2004) Isotopic provinces, mechanism of generation and sources of the continental curst in the Central Asian mobile belt: geological and isotopic evidence. J Asian Earth Sci 23:605–627

Kulp JL, Engels J (1963) Discordance in K–Ar and Rb–Sr isotopic ages. Int. Atomic Energy Agency, Vienna. Radioactive Dating, pp 219–238

Laurent-Charvet S, Charvet J, Monié P, Shu LS (2003) Late Paleozoic strike-slip shear zones in eastern Central Asia (NW China): new structural and geochronological data. Tectonics 22:1099–1101. doi:10.1029/2001TC901047

Li HQ, Xie CF, Chang HL, Cai H, Zhu JP, Zhou S (1998) Study on metallogenetic chronology of nonferrous and precious metallic ore deposits in north Xinjiang, China (in Chinese with English abstract). Geology Publishing House, Beijing, pp 100–127

Li X, Wu X (1996) Late Paleozoic phytogeographic provinces in China and its adjacent regions. Rev Palaeobot Palynol 90:41–62

Li X-P, Zhang LF, Ai YL, Qu JF, Song B, Liu XM (2005a) Zircons overprinted by rodingitization and their U–Pb ages from a serpentinite complex, western Tianshan. Abstr 7th Int Eclog Conf Austria, Mitt Österr Miner Ges 150: p 87

Li YJ, Sun LD, Wu HR, Wang GL, Yang CS, Peng GX (2005b) Permo-Carboniferous radiolaria from the Wupatarkan Group, west terminal of Chinese South Tianshan (in Chinese with English abstract). China J Geol 40:220–226

Li X-P, Zhang LF, Wei CJ, Ai YL, Chen J (2007) Petrology of rodingite derived from eclogite in western Tianshan, China. J Metam Geol 25:363–382. doi:10.1111/j.1525-1314.2007.00700.x

Lin W, Enami M (2006) Prograde pressure-temperature path of jadeite-bearing eclogites and associated high-pressure/low-temperature rocks from western Tianshan, northwest China. Isl Arc 15:477–496. doi:10.1111/j.1440-1738.2006.00545.x

Liu J, Zheng M, Cook NJ, Long X, Deng J, Zhai Y (2007) Geological and geochemical characteristics of the Sawaya'erdun gold deposit, southwestern Chinese Tianshan. Ore Geol Rev 32:125–156. doi:10.1016/j.oregeorev.2006.11.003

Lyons JJ, Coe RS, Zhao X, Renne PR, Kazansky AY, Izokh AE, Kungurtsev LV, Mitrokhin DV (2002) Paleomagnetism of the early Triassic Semeitau igneous series, eastern Kazakstan. J Geophys Res 107:2139. doi:10.1029/2001JB000521

Ludwig KR (2003) Isoplot/Ex version 3. A geochronological toolkit for Microsoft Excel. Berkeley Geochronlogy Center, Spec Publ, vol 4, pp 1–71

Ma RS, Wang CY, Ye SF (1993) Tectonic framework and crustal evolution of Eastern Tianshan Mountains (in Chinese with English abstract). Publishing House of Nanjing University, Nanjing, pp 1–225

Mao JW, Goldfarb RJ, Seltmann R, Wang D, Xiao WJ, Hart C (eds) (2004a) Tectonic evolution and metallogeny of the Chinese Altay and Tianshan Museum of Natural History, London, 282 pp

Mao JW, Konopelko D, Seltmann R, Lehmann B, Chen W, Wang Y, Eklund O, Usubaliev T (2004b) Postcollisional age of the Kumtor Gold deposit and timing of Hercynian events in the Tien Shan, Kyrgyzstan. Econ Geol Bull Soc Econ Geol 99:1771–1780

Mao JW, Goldfarb RJ, Wang Y, Hart CJ, Wang Z, Yang J (2005) Late Paleozoic base and precious metal deposits, East Tianshan, Xinjiang, China: characteristics and geodynamic setting. Episodes 28:23–v36

Mao JW, Pirajno F, Zhang ZH, Chai FM, Wu H, Chen SP, Cheng SL, Yang JM, Zhang C (2008) Late Hercynian post-collisional Cu–Ni sulphide deposits in the Chinese Tianshan and Altay orogens (Xinjiang Province): principal characteristics and ore-forming processes. J

Asian Earth Sci 32:184–203. doi: 10.1016/j.jseaes.2007.10.006

Miller WM, Fallick AE, Leake BE, Macintyre RM, Jenkin GRT (1991) Fluid disturbed hornblende K–Ar ages from the Dalradian rocks of Connemara, Western Ireland. J Geol Soc Lond 148:985–992

Molnar P, Tapponnier P (1975) Cenozoic tectonics of Asia: effects of a continental collision. Science 189:419–426

Pirajno F, Mao JW, Zhang ZC, Zhang ZH, Chai FM (2008) The association of mafic-ultramafic intrusions and A-type magmatism in the Tian Shan and Altay orogens, NW China: implications for geodynamic evolution and potential for the discovery of new ore deposits. J Asian Earth Sci 32:165–183. doi:10.1016/j.jseaes.2007.10.012

Poupinet G, Avouac JP, Jiang M, Wei S, Kissling E, Herquel G, Guilbert J, Paul A, Wittlinger G, Su H, Thomas JC (2002) Intracontinental subduction and Palaeozoic inheritance of the lithosphere suggested by a teleseismic experiment across the Chinese Tien Shan. Terra Nova 14:18–24

Qian Q, Gao J, Klemd R, He G, Xiong XM, Long LL, Liu DY, Xu RH (2008) Early Paleozoic tectonic evolution of the Chinese South Tianshan Orogen: constraints from SHRIMP zircon U–Pb geochronology and geochemistry of basaltic and dioritic rocks from Xiate, NW China. Int J Earth Sci (in press). doi:10.1007/s00531-007-0268-x

Rasmussen B (2005) Zircon growth in very low grade metasedimentary rocks: evidence for zirconium mobility at 250°C? Contrib Mineral Petrol 150:146–155. doi:10.1007/s00410-005-0006-y

Renne PR, Swisher CC, Deino AL, Karner DB, Owens TL, DePaolo DJ (1998) Intercalibration of standards, absolute ages and uncertainties in $^{40}Ar/^{39}Ar$ dating. Chem Geol 145:117–152

Rubin JN, Henry CD, Price JG (1989) Hydrothermal zircons and zircon overgrowths, Sierra Blanca Peaks, Texas. Am Mineral 74:865–869

Rubin JN, Henry CD, Price JG (1993) The mobility of zirconium and other ‘‘immobile’’ elements during hydrothermal alteration. Chem Geol 110:29–47. doi:10.1016/0009-2541(93)90246-F

Ruffet G, Féraud G, Amouric M (1991) Comparison of $^{40}Ar–^{39}Ar$ conventional and laser dating of biotites from the North Trégor Batholith. Geochim Cosmochim Acta 55:1675–1688

Ruffet G, Féraud G, Ballèvre M, Kiénast JR (1995) Plateau ages and excess argon in phengites: an $^{40}Ar–^{39}Ar$ laser probe study of Alpine micas (Sesia zone, Western Alps, northern Italy). Chem Geol 121:327–343

Ruffet G, Gruau G, Ballèvre M, Féraud G, Philippot P (1997) Rb–Sr and ^{40}Ar–^{39}Ar laser probe dating of high-pressure phengites from the Sesia zone (Western Alps): underscoring of excess argon and new age constraints on the high-pressure metamorphism. Chem Geol 141:1–18

Rui Z, Goldfarb RJ, Qiu Y, Zhou T, Chen R, Pirajno F, Yun G (2002) Paleozoic–early Mesozoic gold deposits of the Xinjiang Autonomous Region, northwestern China. Mineral Depos 37:393–418

Shi YS, Lu HF, Jia D, Howell DG (1994) Paleozoic plate tectonic evolution of the Tarim and western Tianshan regions, Western China. Int Geol Rev 36:1058–1066

Shu LS, Charvet J, Guo LZ, Lu HF, Laurent-Charvet S (1999) A large-scale Palaeozoic dextral ductile strike-slip zone: the Aqqikkudug-Weiya zone along the northern margin of the Central Tianshan belt, Xinjiang, NW China. Acta Geol Sin 73:148–162

Shu LS, Lu HF, Charvet J, Laurent-Charvet S, Yin DH (2000) Paleozoic accretionary terranes in Northern Tianshan, NW China. Chin Geochem 19:193–202

Shu LS, Charvet J, Lu HF, Laurent-Charvet S (2002) Paleozoic accretion-collision events and kinematics of ductile deformation in the central-southern Tianshan Belt, China. Acta Geol Sin 76:308–323

Shu LS, Zhu WB, Wang B, Faure M, Charvet J, Cluzel D (2005) The post-collision intracontinental rifting and olistostrome on the southern slope of Bogda Mountains, Xinjiang (in Chinese with English abstract). Acta Petrol Sin 21:25–36

Sibson RH (1987) Earthquake rupturing as a mineralizing agent in hydrothermal systems. Geology 15:701–704

Sibson RH (2007) Au-quartz mineralization near the base of the continental seismogenic zone. In: Ries AC, Butler RWH, Graham RH (eds) Deformation of the Continental Crust: the Legacy of Mike Coward. Geol Soc Lond Spec Publ, vol 272, pp 519–532

Sisson VB, Onstott TC (1986) Dating blueschist metamorphism: a combined $^{40}Ar/^{39}Ar$ and electron microprobe approach. Geochim Cosmochim Acta 50:2111–2117

Steiger RH, Jäger E (1977) Subcommission on geochronology: convention on the use of decay constants in geo- and cosmology. Earth Planet Sci Lett 36:359–362

Stupakov SI, Volkova NI, Travin AV, Simonov A, Sakiev KS, Novgorodtsev OS (2004) Eclogites of Atbashi Ridge as indicators of Early Carboniferous collision in Southern Tien Shan. In: Chernyshov AI, Tishin PA, Bether OV, Vrublevsky VV, Gertner IF, Grinev OM, Krasnova TS (eds) Petrology of magmatic and metamorphic complexes. Issue 4, Tomsk Center for Scientific and Technical Information, pp 272–277 (in Russian)

Tagiri M, Yano T, Bakirov A, Nakajima T, Uchiumi S (1995) Mineral parageneses and metamorphic P-T paths of ultrahigh-pressure eclogites from Kyrghyzstan Tien-Shan. Isl Arc

4:280–292

Tsygankov AA, Matukov DI, Berezhnaya NG, Larionov AN, Posokhov VF, Tsyrenov BT, Khromov AA, Sergeev SA (2007) Late Paleozoic granitoids of western Transbaikalia: magma sources and stages of formation. Russ Geol Geoph 48:120–140. doi:10.1016/j.rgg.2006.12.011

Volkova NI, Budanov VI (1999) Geochemical discrimination of metabasalt rocks of the Fan–Karategin transitional blueschist/greenschist belt, South Tianshan, Tajikistan: seamount volcanism and accretionary tectonics. Lithos 47:201–216

Volkova NI, Sklyarov EV (2007) High-pressure complexes of Central Asian Fold Belt: geologic setting, geochemistry, and geodynamic implications. Russ Geol Geoph 48:83–90. doi:10.1016/j.rgg.2006.12.008

Walther JV (1994) Fluid-rock reactions during metamorphism at mid-crustal conditions. J Geol 102:559–570

Wang B (2006) Paleozoic geodynamic evolution of Yili Block in West Chinese Tianshan. PhD thesis, University of Orleans, Orléans, France, pp 1–244 (in French and Chinese, with English abstract). http://tel.archives-ouvertes.fr/tel-00140948/en/

Wang Y, Mooney WD, Yuan X, Coleman RG (2003) The crustal structure from the Altai mountains to the Altyn Tagh fault, northwest China. J Geoph Res 108(B6):2322. doi:10.1029/2001JB000552

Wang B, Faure M, Cluzel D, Shu LS, Charvet J, Meffre S, Ma Q (2006) Late Paleozoic tectonic evolution of the northern West Chinese Tianshan Belt. Geod Acta 19:227–237

Wang B, Chen Y, Zhan S, Shu LS, Faure M, Cluzel D, Charvet J, Laurent-Charvet S (2007a) Primary Carboniferous and Permian paleomagnetic results from the Yili Block (NW China) and their geodynamic implications on the evolution of Chinese Tianshan Belt. Earth Planet Sci Lett 263:288–308

Wang B, Shu LS, Cluzel D, Faure M, Charvet J (2007b) Geochemical constraints on Carboniferous volcanic rocks of Yili Block (Xinjiang, NW China): implication on tectonic evolution of Western Tianshan. J Asian Earth Sci 29:148–159

Wang B, Cluzel D, Shu LS, Faure M, Chen, Y, Meffre S, Charvet J, de Jong K (2008a) Persistence and evolution of calc-alkaline to alkaline magmatism through changing geodynamic setting: from Carboniferous convergence to Permian transcurrent tectonics, western Chinese Tianshan. In: Xiao WJ, Kröner A, Windley BF (eds) Geodynamic evolution of Central Asia in the Paleozoic and Mesozoic. Int J Earth Sci (accepted)

Wang B, Faure M, Shu LS, Cluzel D, Charvet J, de Jong K, Chen Y (2008b) Paleozoic tectonic evolution of the Yili Block, Western Chinese Tianshan. Bull Soc Géol Fr (in press)

Wang B, Faure M, Shu LS, de Jong K, Cluzel D, Charvet J, Meffre S, Ruffet G, Chen Y (2008c) Tectonics of the Yili Block in the southern part of the Western Chinese Tianshan, and its Paleozoic geodynamic evolution. Tectonics (submitted)

Wei CJ, Powell R, Zhang LF (2003) Eclogites from the south Tianshan, NW China: petrological characteristic and calculated mineral equilibria in the Na_2O–CaO–FeO–MgO–Al_2O_3–SiO_2–H_2O system. J Metam Geol 21:169–179

Wilde AR, Layer P, Mernagh T, Foster J (2001) The giant Muruntau gold deposit: geologic, geochronologic, and fluid inclusion constraints on ore genesis. Econ Geol 96:633–644. doi:10.2113/96.3.633

Windley BF, Allen MB, Zhang C, Zhao ZY, Wang GR (1990) Paleozoic accretion and Cenozoic redeformation of the Chinese Tien Shan range, Central Asia. Geology 18:128–131

Windley BF, Alexeiev D, Xiao WJ, Kröner A, Badarch G (2007) Tectonic models for accretion of the Central Asian Orogenic Belt. J Geol Soc Lond 164:31–47

Wu FY, Sun DY, Li H, Jahn BM, Wilde S (2002) A-type granites in northeastern China: age and geochemical constraints on their petrogenesis. Chem Geol 187:143–173

XBGMR (Xinjiang Bureau of Geology and Mineral Resources) (1993) Regional geology of Xinjiang Uygur Autonomy Region (in Chinese with English abstract). Geology Publishing House, Beijing, pp 1–841

Xiao WJ, Windley BF, Hao J, Zhai M (2003) Accretion leading to collision and the Permian Solonker Suture, Inner Mongolia, China: termination of the Central Asian Orogenic Belt. Tectonics 22:1069–1089. doi:10.1029/2002TC001484

Xiao WJ, Zhang LC, Qin KH, Sun S, Li JL (2004) Paleozoic accretionary and collisional tectonics of the eastern Tienshan (China): implications for the continental growth of Central Asia. Am J Sci 304:370–395

Xiao WJ, Han CM, Yuan C, Sun M, Lin SF, Chen HL, Li ZL, Li JL, Sun S (2008a) Middle Cambrian to Permian subduction-related accretionary orogenesis of Northern Xinjiang, NW China: implications for the tectonic evolution of central Asia. J Asian Earth Sci 32:102–117. doi:10.1016/j.jseaes.2007.10.008

Xiao WJ, Windley BF, Han CM, Yuan C, Chen HL, Sun M, Sun S Li JL (2008b) End-Permian to Triassic termination of the accretionary process in southern Altaids: implications for the geodynamic evolution, the Phanerozoic continental growth, and metallogeny of Central Asia. In: Xiao WJ, Kröner A, Windley BF (eds) Geodynamic evolution of Central Asia in the Paleozoic and Mesozoic. Int J Earth Sci (accepted)

Xiao XC, Tang YQ, Feng YM, Zhu BQ, Li JY, Zhao M (1992) Tectonic evolution of the northern Xinjiang and its adjacent regions (in Chinese with English abstract). Geology Publishing House, Beijing, pp 1–169

Yakubchuk A (2004) Architecture and mineral deposit settings of the Altaid orogenic collage: a revised model. J Asian Earth Sci 23:761–779

Yakubchuk AS, Cole A, Seltmann R, Shatov VV (2002) Tectonic setting, characteristics, and regional exploration criteria for gold mineralization in the Altaid orogenic collage: the Tien Shan province as a key example. Soc Econ Geol Spec Publ 9:177–201

Yang FQ, Mao JW, Wang Y, Bierlein FP (2006) Geology and geochemistry of the Bulong quartz-barite vein-type gold deposit in the Xinjiang Uygur Autonomous Region, China. Ore Geol Rev 29:52–76

Zack T, John T (2007) An evaluation of reactive fluid flow and trace element mobility in subducting slabs. Chem Geol 239:199–216. doi:10.1016/j.chemgeo.2006.10.020

Zhang LC, Shen YC, Ji JS (2003) Characteristics and genesis of Kanggur gold deposit in the eastern Tianshan mountains, NW China: evidence from geology, isotope distribution and chronology. Ore Geol Rev 23:71–90

Zhang LF, Ai YL, Li XP, Rubatto D, Song B, Williams S, Song SG, Ellis D, Liou JG (2007) Triassic collision of western Tianshan orogenic belt, China: Evidence from SHRIMP U–Pb dating of zircon from HP/UHP eclogitic rocks. Lithos 96:266–280. doi:10.1016/j.lithos.2006.09.012

Zhang LC, Qin KH, Xiao WJ (2008a) Multiple mineralization events in the eastern Tianshan district, NW China: isotopic geochronology and geological significance. J Asian Earth Sci 32:236–246. doi:10.1016/j.jseaes.2007.10.011

Zhang ZH, Mao JW, Du AD, Pirajno F, Wang ZL, Chai FM, Zhang ZC, Yang JM (2008b) Re–Os dating of two Cu-Ni sulfide deposits in northern Xinjiang and its geological significance. J Asian Earth Sci 32:204–217. doi:10.1016/j.jseaes.2007.10.005

Zhao JM, Liu GD, Lu ZX, Zhang XK, Zhao GZ (2003) Lithospheric structure and dynamic processes of the Tianshan orogenic belt and the Junggar basin. Tectonoph 376:199–239

Zhao ZH, Xiong XL, Wang Q, Wyman DA, Bao ZW, Bai ZH, Qiao YL (2008) Underplating-related adakites in Xinjiang Tianshan, China. Lithos 102:374–391. doi:10.1016/j.lithos.2007.06.008

Zheng JP, Luo ZH, Yu CM, Yu XL, Zhang RS, Lu FX, Li HM (2005) Geochemistry and zircon U–Pb ages of granulite xenolith from Tuoyun basalts, Xinjiang: Implications for the petrogenesis and the lower crustal nature beneath the southwestern Tianshan. Chin Sci Bull 50:1242–1251

Zhou D, Graham SA, Chang EZ, Wang BY, Hacker B (2001) Paleozoic tectonic amalgamation of the Chinese Tianshan: evidence from a transect along the Dushanzi-Kuqa highway. In: Hendrix MS, Davis GA (eds) Paleozoic and Mesozoic tectonic evolution of central Asia: from continental assembly to intracontinental deformation. Geol Soc Am Mem, vol 194, Boulder, pp 23–46

Zhou MF, Lesher CM, Yang ZX, Li JW, Sun M (2004) Geochemistry and petrogenesis of 270 Ma Ni-Cu-(PGE) sulfide-bearing mafic intrusions in the Huangshan district, Eastern Xinjiang, Northwestern China: Implication for the tectonic evolution of the Central Asian

orogenic belt. Chem Geol 209:233–257. doi:10.1016/j.chemgeo.2004.05.005

Zhou TF, Yuan F, Tan LG, Fan Y, Yue SC (2006) Geodynamic significance of the A-type granites in the Sawuer region in west Junggar, Xinjiang: rock geochemistry and SHRIMP zircon age evidence. Sci Chin Ser D Earth Sci 49:113–123. doi:10.1007/s11430-005-0121-7

Zhu Y, Zhou J, Zeng Y (2006) The Tianger (Bingdaban) shear zone hosted gold deposit, west Tianshan, NW China: Petrographic and geochemical characteristics. Ore Geol Rev 32:337–365. doi:10.1016/j.oregeorev.2006.10.006

Figures

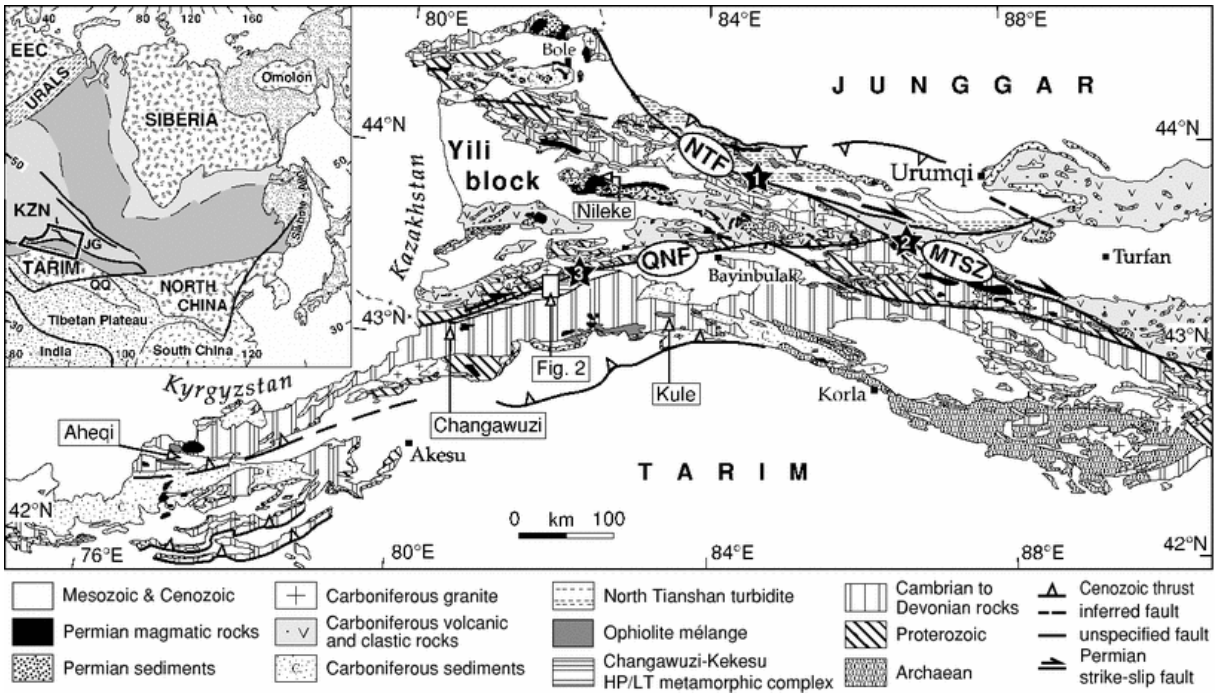

Fig. 1 Geological sketch map of the Chinese Tianshan Belt (modified after: Hu et al. *2000*; Wang *2006*; Wang et al. *2008a*, this issue) that is tectonically subdivided into distinct provinces along a number of trans-crustal strike-slip faults active since Early Permian time. Mentioned in the text are: *NTF* North Tianshan Fault, *MTSZ* Main Tianshan Shear Zone, *QNF* Qingbulak-Nalati Fault. Samples indicated by numbered stars; *1* XJ628−7, *2* XJ703, *3* XJ620. The sampling area along the Kekesu River south of the Qingbulak-Nalati strike-slip fault (Fig. 2) is indicated. *Inset* (modified after Jahn *2004*; de Jong et al. *2006*; Wang et al. *2007a*) shows the location of the study area within the tectonic framework of Central Asia. The Central Asian Orogenic Belt has a *dark shading*; cratons have a light hatching; Kazakhstan (*light shading*) is regarded as a composite continent or a terrane assemblage formed by amalgamated microcontinental fragments with Proterozoic basement and volcanic arcs, separated by Palaeozoic subduction–accretion complexes (Filippova et al. *2001*; Windley et al. *2007*; Cocks and Torsvik *2007*). *EEC* East European Craton, *KZN* Kazakhstan Continent, *JG* Junggar Block, *QQ* Qiadam Qinling

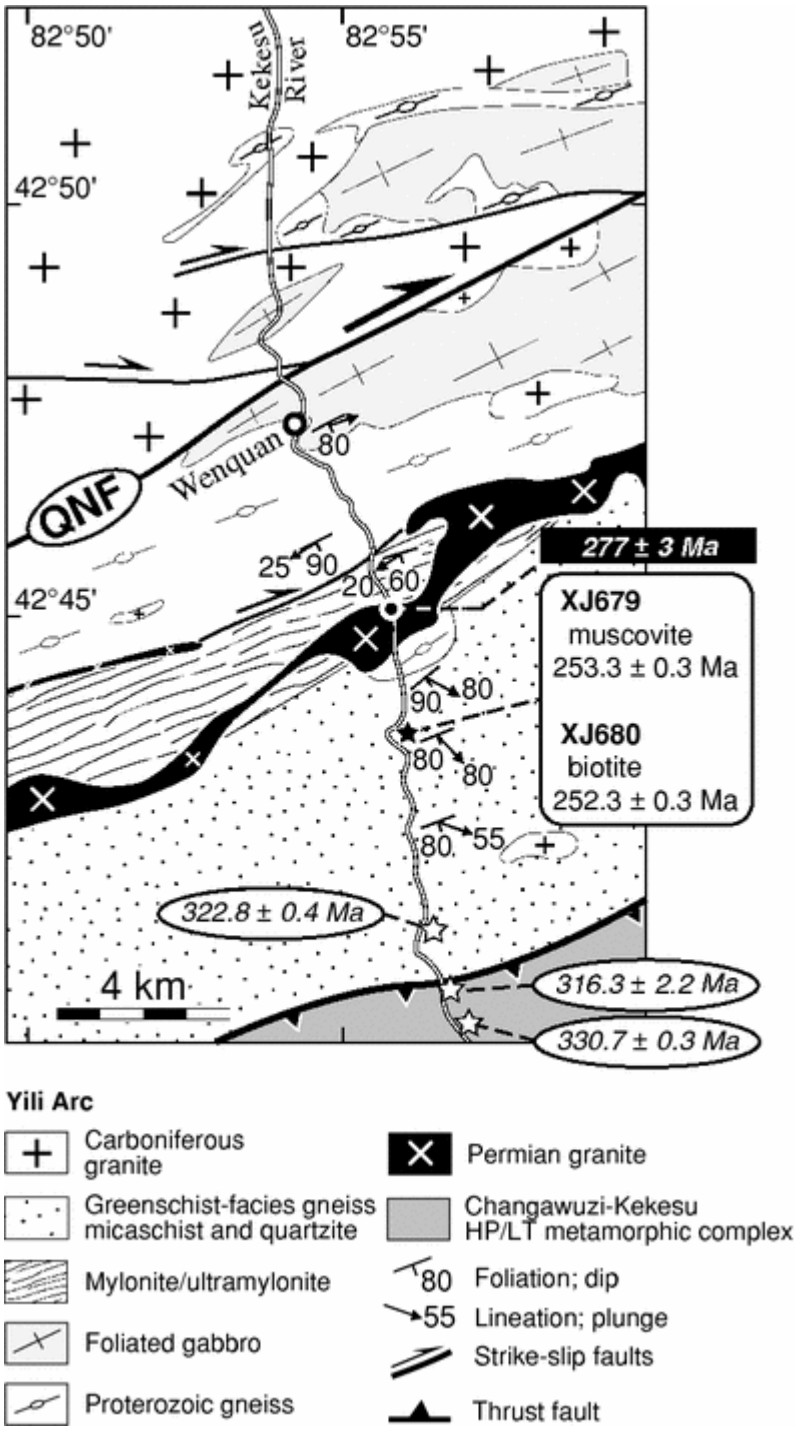

Fig. 2 Geological map of the southern margin of the Yili arc along the Kekesu River (after: Wang et al. *2008c*; map area indicated in Fig. 1), along which samples XJ679 and XJ680 (indicated by *black star*) have been collected. White mica $^{40}Ar/^{39}Ar$ plateau ages in italics in ellipses are from Wang et al. (*2008c*). The strongest retrogressed blueschist that gave the youngest $^{40}Ar/^{39}Ar$ age of 316.3 ± 2.2 Ma was taken immediately above the basal thrust fault of the Changawuzi-Kekesu belt. White mica in greenschist-facies metamorphic quartzite from the ductilely deformed metasedimentary cover of the crystalline basement, taken at about 1 km below the thrust contact with the Changawuzi-Kekesu belt, gave a plateau age of 322.8 ± 0.4 Ma. *Solid square* zircon U–Pb LA-ICPMS weighted mean age (277±3 Ma) of the Kekesu K-granite (sample KKS5 of Wang et al. *2008a*, this issue). Please note the differences in structural styles of the pre-Carboniferous basement of gabbros, mylonites and Proterozoic

gneisses, characterised by ductile deformation fabrics with weakly plunging lineations, and its greenschist-facies metasedimentary cover with steeply plunging lineations. The Kekesu granite intruded along this basement-cover contact. A number of splays occur on both sides of the dextral Permian Qingbulak-Nalati strike-slip fault (*QNF*) that seems to be in part used by the Early Permian granite intrusion

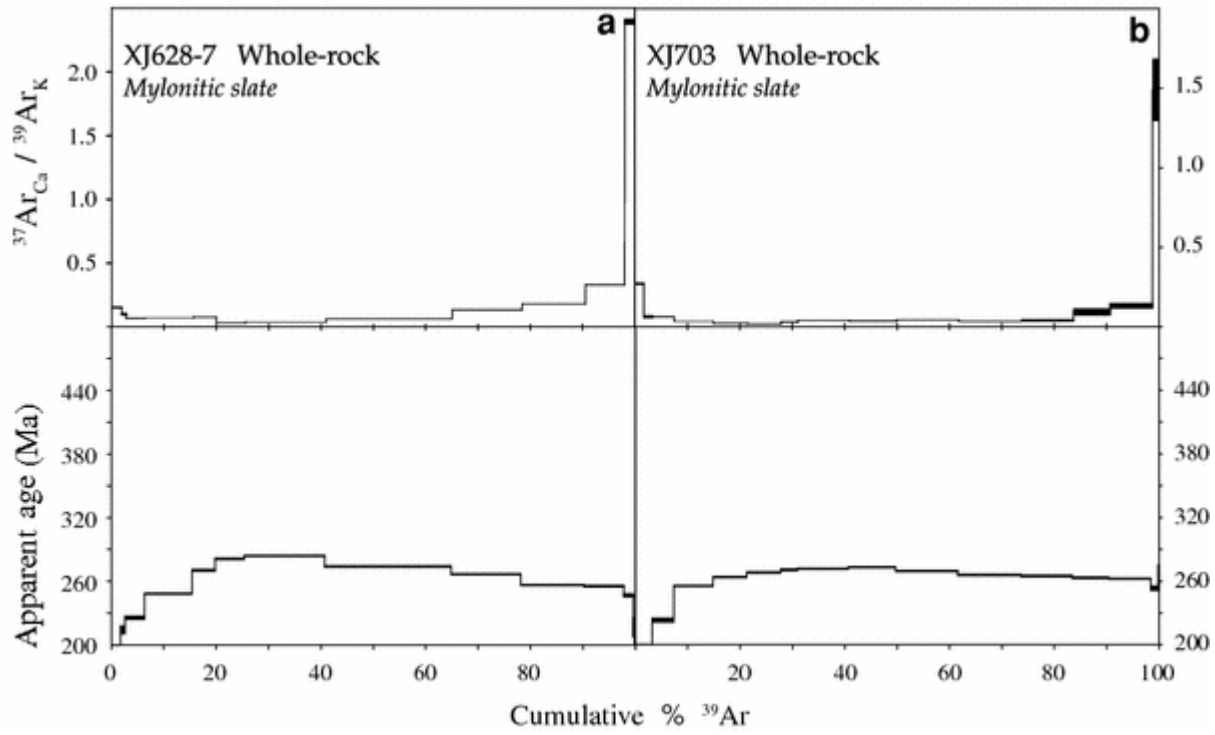

Fig. 3 $^{40}Ar/^{39}Ar$ age spectra acquired by laser step heating of whole-rock single fragments of mylonitic slates XJ628-7 from the North Tianshan Fault (**a**) and XJ703 from the Main Tianshan Shear Zone (**b**)

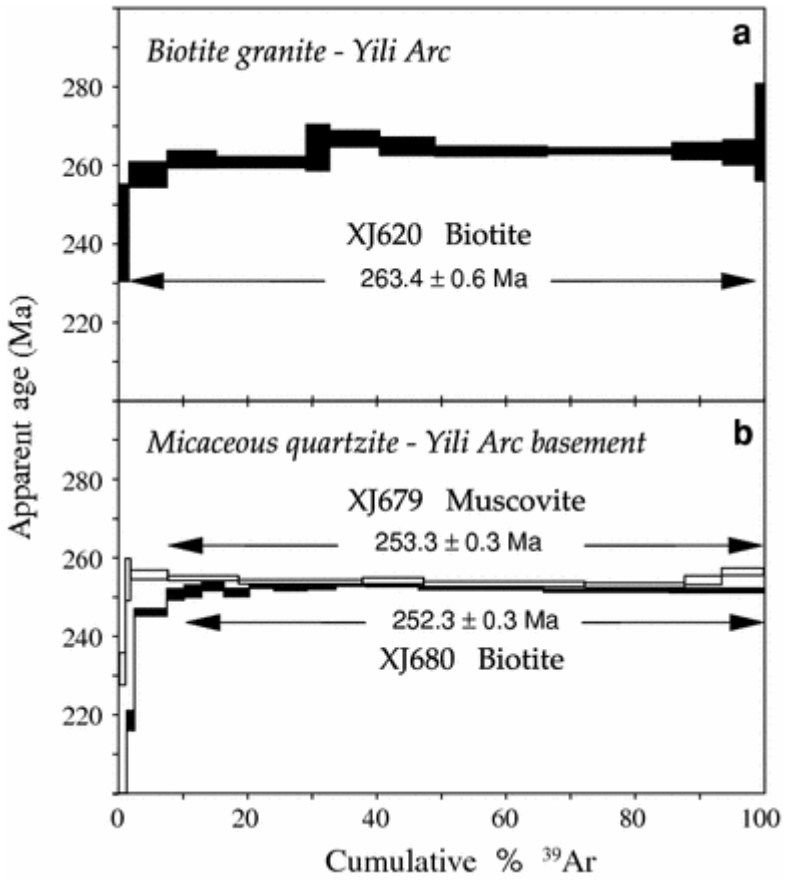

Fig. 4 $^{40}Ar/^{39}Ar$ age spectra acquired by laser step heating of a biotite single grain XJ620 from a Carboniferous biotite granite of the Yili arc (**a**) and muscovite XJ679 and biotite XJ680 (**b**) single grains from micaceous quartzites from the metamorphosed and ductilely deformed sedimentary cover of the crystalline basement of the southern margin of the Yili arc

Table

Table 1 $^{40}Ar/^{39}Ar$ analytical data of laser step heating of mica single grains and whole-rock single fragments from the western Tianshan

Step	**$^{40}Ar_{Atm}$ (%)**	**$^{39}Ar_K$ (%)**	**$^{37}Ar_{Ca}/^{39}Ar_K$**	**$^{40}Ar^*/^{39}Ar_K$**	**Apparent age and error (Ma)**
XJ620	**Biotite**	**Carboniferous biotite granite Yili Arc**		***J* = 0.00539451**	
1	17.4	1.6	3.52E−01	26.74	243.1 ± 12.5
2	8.1	5.9	1.00E−02	28.50	258.0 ± 3.2
3	4.7	7.6	5.30E−02	28.96	261.9 ± 2.2
4	3.3	13.9	6.10E−02	28.87	261.2 ± 1.4
5	2.5	3.6	0.00E+00	29.31	264.8 ± 5.9
6	0.9	7.7	0.00E+00	29.58	267.1 ± 2.1
7	1.7	8.6	6.00E−03	29.34	265.1 ± 2.3
8	1.1	17.3	1.40E−02	29.21	263.9 ± 1.3
9	1.5	19.4	0.00E+00	29.21	264.0 ± 0.8
10	2.1	7.9	1.70E−02	29.20	263.9 ± 2.2
11	2.4	5.0	0.00E+00	29.17	263.6 ± 3.2
Fusion	2.7	1.4	2.60E−02	29.77	268.7 ± 12.4
XJ628-7	**Whole-rock**	**Mylonite North Tianshan Fault**		***J* = 0.00539635**	
1	35.4	1.7	1.75E−01	16.79	156.5 ± 3.7
2	8.1	0.9	1.21E−01	23.35	214.1 ± 3.6
3	2.0	3.7	9.00E−02	24.70	225.7 ± 1.5
4	1.1	9.1	9.10E−02	27.36	248.4 ± 0.5
5	0.5	4.4	9.80E−02	29.96	270.4 ± 0.9
6	0.3	5.6	5.30E−02	31.26	281.3 ± 0.7
7	0.4	15.4	5.90E−02	31.59	284.0 ± 0.5

XJ628-7	Whole-rock	Mylonite North Tianshan Fault		*J* = 0.00539635	
8	0.5	24.1	8.30E−02	30.40	274.1 ± 0.5
9	0.6	13.3	1.54E−01	29.53	266.8 ± 0.5
10	1.0	12.1	2.00E−01	28.33	256.6 ± 0.5
11	0.9	7.5	3.47E−01	28.20	255.5 ± 0.7
12	2.9	1.8	2.39E+00	27.18	246.9 ± 1.3
13	9.1	0.2	7.20E+00	23.64	216.6 ± 9.0
Fusion	65.5	0.2	4.48E+00	10.96	103.7 ± 25.2

XJ679	Muscovite	Micaceous quartzite Yili Basement		*J* = 0.00539735	
1	11.4	1.0	8.00E–03	25.31	231.1 ± 11.4
2	4.7	0.7	1.48E–01	27.99	253.9 ± 4.7
3	6.7	5.9	0.00E+00	28.14	255.1 ± 6.7
4	3.5	10.9	1.20E–02	28.03	254.2 ± 3.5
5	1.7	19.2	2.50E–02	27.94	253.4 ± 1.7
6	0.7	9.5	3.50E–02	27.97	253.7 ± 0.7
7	0.7	24.9	2.30E–02	27.87	252.8 ± 0.7
8	0.7	15.4	3.20E–02	27.82	252.4 ± 0.7
9	0.3	5.7	1.00E–02	27.98	253.8 ± 0.3
Fusion	0.0	6.8	0.00E+00	28.23	255.9 ± 0.0

XJ680	Biotite	Micaceous quartzite Yili Basement		*J* = 0.00539727	
1	86.6	0.7	5.70E–02	7.71	73.5 ± 14.8
2	23.3	0.6	1.40E–01	17.63	163.9 ± 4.6
3	12.6	1.2	4.50E–02	23.87	218.6 ± 2.5
4	3.7	5.0	5.40E–02	27.10	246.2 ± 0.9

XJ680	**Biotite**	**Micaceous quartzite Yili Basement**		***J* = 0.00539727**	
5	1.5	2.7	0.00E+00	27.64	250.8 ± 1.5
6	1.7	2.7	0.00E+00	27.74	251.6 ± 1.6
7	0.7	3.5	0.00E+00	27.89	252.9 ± 1.2
8	1.1	3.9	0.00E+00	27.69	251.3 ± 1.1
9	0.2	3.8	2.50E–02	27.92	253.1 ± 0.8
10	0.6	5.1	2.60E–02	27.83	252.4 ± 0.8
11	0.2	4.4	1.60E–02	27.91	253.1 ± 1.0
12	0.2	4.7	3.40E–02	27.98	253.7 ± 0.7
13	0.6	8.1	4.80E–02	27.93	253.2 ± 0.5
14	0.4	19.3	7.30E–02	27.84	252.5 ± 0.5
15	0.3	19.5	8.10E–02	27.75	251.7 ± 0.5
Fusion	0.4	14.7	1.10E+00	27.76	251.8 ± 0.7

XJ703	**Whole-rock**	**Mylonite MainTianshan Shear Zone**		***J* = 0.00539543**	
1	63.3	1.5	2.87E–01	13.04	122.6 ± 3.3
2	17.5	1.7	8.00E–02	17.20	160.1 ± 1.4
3	6.9	4.1	8.10E–02	24.41	223.2 ± 1.8
4	1.1	7.5	5.30E–02	28.22	255.6 ± 0.5
5	0.6	6.4	4.00E–02	29.22	264.0 ± 0.5
6	0.5	6.5	3.60E–02	29.72	268.3 ± 0.7
7	0.6	3.2	4.80E–02	30.02	270.8 ± 0.9
8	0.5	9.7	5.80E–02	30.15	271.9 ± 0.5
9	0.4	9.1	5.40E–02	30.31	273.2 ± 0.5
10	0.7	11.9	6.00E–02	29.89	269.7 ± 0.5

XJ703	**Whole-rock**	**Mylonite MainTianshan Shear Zone**		***J* = 0.00539543**	
11	0.9	12.0	5.30E–02	29.45	266.0 ± 0.6
12	1.0	9.8	5.90E–02	29.33	265.0 ± 0.6
13	1.3	6.9	1.11E–01	29.12	263.2 ± 0.7
14	1.5	8.1	1.49E–01	29.04	262.5 ± 0.5
15	6.0	1.4	1.49E+00	27.97	253.5 ± 2.0
Fusion	25.2	0.2	6.33E+00	29.13	263.3 ± 12.0